Properties of the superconducting state in a two-band model

E. J. Nicol
Department of Physics, University of Guelph, Guelph, Ontario, NIG 2W1, Canada

J. P. Carbotte
Department of Physics and Astronomy, McMaster University, Hamilton, Ontario, L8S 4M1, Canada
(Received 12 September 2004; published 2 February 2005)

Eliashberg theory is used to investigate the range of thermodynamic properties possible within a two-band model for *s*-wave superconductivity and to identify signatures of its two-band nature. We emphasize dimensionless BCS ratios [those for the energy gaps, the specific heat jump, and the negative of its slope near T_c, the thermodynamic critical field $H_c(0)$, and the normalized slopes of the critical field and the penetration depth near T_c], which are no longer universal even in weak coupling. We also give results for temperature-dependent quantities, such as the penetration depth and the energy gap. Results are presented both for microscopic parameters appropriate to MgB_2 and for variations away from these. Strong coupling corrections are identified and found to be significant. Analytic formulas are provided that show the role played by the anisotropy in coupling in some special limits. Particular emphasis is placed on small interband coupling and on the opposite limit of no diagonal coupling. The effect of impurity scattering is considered, particularly for the interband case.

DOI: 10.1103/PhysRevB.71.054501 PACS number(s): 74.20−z, 74.70.Ad, 74.25.Bt, 74.25.Nf

I. INTRODUCTION

The properties of the superconducting state of conventional, single-band, electron-phonon superconductors differ markedly from BCS predictions.[1] However, they are well-described within isotropic Eliashberg theory with a single electron-phonon spectral density $\alpha^2F(\omega)$ for the average interaction over the Fermi surface. This function is accurately known from inversion of tunneling data.[2] In many cases, $\alpha^2F(\omega)$ has also been calculated from first-principle electronic band structure calculations extended to include the electron-phonon interaction, sometimes with the phonons taken directly from inelastic neutron scattering measurements. In many cases, such results agree very well with the corresponding tunneling data. While it is to be noted that, in principle, the electron-phonon spectral density for the various electrons on the Fermi surface is anisotropic leading to energy gap anisotropy,[3–6] this feature often does not play a prominent role because, in many instances, the electronic mean free path is much smaller than the coherence length. In such circumstances, a Fermi surface average of the electron-phonon spectral density can be used. Nevertheless, corrections due to gap anisotropy have been identified and studied in the past,[7] often, but not always, in a separable anisotropic model.[8]

The history of two-band superconductivity[9–12] and of MgB_2 [with $T_c \simeq 39$ K (Ref. 13)] in particular[14–22] is somewhat different. To our knowledge, as yet, there exists no inversion[23] of tunneling data from which the electron-phonon interaction is determined. In fact, it has been noted[24] that this may well never be possible in MgB_2 because of its two-band nature, which requires a microscopic description in terms of four separate electron-phonon spectral functions $\alpha_{ij}^2F(\omega)$, where $i=\sigma,\pi$ (or 1,2), with the two-dimensional σ band having the largest electron-phonon coupling. The three-dimensional π band on its own would have a smaller value of T_c, the critical temperature, although it has a higher value of the electron density of states at the Fermi energy.

In the absence of tunneling data giving reliable information on the fundamental kernels entering the two-band Eliashberg equations, first-principle band structure calculations of $\alpha_{ij}^2F(\omega)$ in MgB_2 have been used to compute superconducting properties (for example, Refs. 16–19). To do this, it is also necessary to know the Coulomb pseudopotential repulsions μ_{ij}^*, which are different for various indices (i,j), but these have also been calculated. Good agreement with experiment is obtained in this way for the properties considered so far, more explicitly, the specific heat,[16,25] the penetration depth,[17,26] and the anisotropy in the two gaps, as well as their temperature dependence. For the penetration depth, impurity scattering can be important, and in- and out-of-plane orientations of the magnetic field are different.[17]

In this paper, we use the band theory information on $\alpha_{ij}^2F(\omega)$ and μ_{ij}^* in MgB_2 to calculate the critical temperature, the energy gap with its anisotropy and temperature dependence, and other thermodynamic properties, as well as the penetration depth, giving particular emphasis to strong coupling corrections. Further to our discussion of MgB_2, we provide a full listing of calculated dimensionless BCS ratios, now modified by both the anisotropy and the strong coupling effects in MgB_2, and make comparison with experiment. We also consider effects of variations in microscopic parameters away from those of MgB_2, as well as impurity scattering—intraband and interband. To this end, we reduce the two-band Eliashberg equations, which fully account for retardation, in the two-square-well approximation (also called the $\lambda^{\theta\theta}$ model). This leads to simple *renormalized* BCS (RBCS) forms, which, when compared to our full numerical Eliashberg results, allow us to identify the strong coupling corrections that we find to be significant even for MgB_2.

When considering variations in microscopic parameters away from those of MgB_2, we place particular emphasis on two limiting cases: the limit of small interband coupling and the opposite case, when the intraband coupling is zero and the superconductivity is due to the interband coupling alone, a case discussed in the early work of Shul *et al.*[9] We also consider the special case when the intraband coupling in the second band is repulsive. The limit of small interband coupling is particularly interesting because it allows us to understand how the off-diagonal terms lead to the integration of otherwise two completely independent and noncommunicating superconducting bands with separate transition temperatures T_{ci}. In this regard, we find that $\alpha_{12}^2F(\omega)$ and $\alpha_{21}^2F(\omega)$ behave very differently, with 21 the most effective variable at integrating the two systems and 12 the most effective at changing the critical temperature. The presence of the off-diagonal interactions rapidly smear out the features of the second transition at T_{c2}, i.e., the one with the smaller of the two T_{ci} values. More specifically, surprisingly small values of the mass renormalization parameter λ_{21}, as compared with λ_{11} and λ_{22}, have a large effect on the region of T_{c2}. We also find that relatively modest values of the interband impurity scattering rates lead to the significant integration of the two bands. Even when the bands are well-integrated, in the sense that little trace of a second sharp transition at T_{c2} remains, there still exist important modifications of the usual one-band BCS results because of the two distinct bands. As an example, the BCS dimensionless universal ratios now depend on the ratio of the electronic density of states at the Fermi energy of the two bands. Simple analytic expressions for these ratios are derived, which provide insight into the physics underlying two-band superconductivity and guidance as to how these results are to be interpreted.

In Sec. II, we give the two-band Eliashberg equations and provide their reduction in the $\lambda^{\theta\theta}$ approximation, which is needed to identify strong coupling corrections to renormalized two-band BCS (RBCS). Section III deals with the dependence of T_c on microscopic parameters, i.e., on the electron-phonon interaction as well as on impurities. Intra- and interband quantities are both of interest. We consider modifications of the dimensionless BCS ratios in the $\lambda^{\theta\theta}$ model, as well as the zero-temperature value of the two gaps and their anisotropy. MgB_2 is considered in Sec. IV. The issue of strong coupling corrections in MgB_2, and more generally in other related systems, is discussed. The limit of small interband electron-phonon coupling is considered in Sec. V. We study, in particular, how the two otherwise separate bands become integrated when this interaction is switched on. The effect of interband impurity scattering is also considered in the same context as it exhibits analogous behavior to the case of the off-diagonal electron-phonon coupling. In Sec. VI, we deal briefly with the less realistic case of zero intraband electron-phonon coupling, where the superconductivity is due only to the interband piece. Conclusions are found in Sec. VII.

Finally, in light of the recent developments in other areas of superconductivity and correlated electrons, we wish to emphasize that our use of the term "gap anisotropy" here is in reference to the difference in the magnitudes of the two gaps, each of which are isotropic *s* wave in this work, and hence does not refer to a momentum-dependent order parameter. Likewise, "strong coupling" refers to the traditional meaning of strong electron-phonon coupling and is not an allusion to strong interband coupling.

II. THEORY

The isotropic (within a band) Eliashberg equations generalized to two bands ($i=1,2$) are written on the imaginary axis as[12,1,3,4]

$$\Delta_i(i\omega_n)Z_i(i\omega_n) = \pi T\sum_m\sum_j [\lambda_{ij}(i\omega_m - i\omega_n) - \mu_{ij}^*(\omega_c)\theta(\omega_c - |\omega_m|)]\frac{\Delta_j(i\omega_m)}{\sqrt{\omega_m^2 + \Delta_j^2(i\omega_m)}} + \pi\sum_j (t_{ij}^+ - t_{ij}^-)\frac{\Delta_j(i\omega_n)}{\sqrt{\omega_n^2 + \Delta_j^2(i\omega_n)}} \quad (1)$$

and

$$Z_i(i\omega_n) = 1 + \frac{\pi T}{\omega_n}\sum_m\sum_j \lambda_{ij}(i\omega_m - i\omega_n)\frac{\omega_m}{\sqrt{\omega_m^2 + \Delta_j^2(i\omega_m)}} + \pi\sum_j (t_{ij}^+ + t_{ij}^-)\frac{\omega_n}{\sqrt{\omega_n^2 + \Delta_j^2(i\omega_n)}}, \quad (2)$$

where $t_{ij}^+ = 1/(2\pi\tau_{ij}^+)$ and $t_{ij}^- = 1/(2\pi\tau_{ij}^-)$ are the ordinary and paramagnetic impurity scattering rates, respectively, and

$$\lambda_{ij}(i\omega_m - i\omega_n) \equiv 2\int_0^\infty \frac{\Omega\alpha^2F_{ij}(\Omega)}{\Omega^2 + (\omega_n - \omega_m)^2}d\Omega. \quad (3)$$

Equation (1) gives the gap $\Delta_i(i\omega_n)$ and Eq. (2) the renormalization $Z_i(i\omega_n)$ at the nth Matsubara frequency $i\omega_n$, with $\omega_n = (2n-1)\pi T$. Here, T is temperature and $n=0,\pm1,\pm2,\ldots$. The electron-phonon kernels are $\alpha_{ij}^2F(\Omega)$ as a function of phonon energy Ω and the Coulomb repulsions are μ_{ij}^*, with a high energy cutoff ω_c needed for convergence and usually taken to be about six to ten times the maximum phonon frequency. For the specific case of MgB_2, these may be found in Ref. 19. The diagonal intraband elements of the electron-phonon interaction are largest, in the case of MgB_2, while the off-diagonal elements describing interband scattering are smaller, but still substantial.

In what is called the two-square-well approximation or $\lambda^{\theta\theta}$ model,[11,27,28] we use in Eq. (1):

$$\lambda_{ij}(i\omega_m - i\omega_n) = \begin{cases} \lambda_{ij} & \text{for both} |\omega_n|, |\omega_m| < \omega_o \\ 0 & \text{otherwise,} \end{cases} \quad (4)$$

where

$$\lambda_{ij}(m=n) = \lambda_{ij}(0) \equiv \lambda_{ij} = 2\int_0^\infty \frac{\alpha^2F_{ij}(\Omega)}{\Omega}d\Omega. \quad (5)$$

Neglecting the gap in the denominator on the right-hand side of Eq. (2) for Z, we further approximate (see Ref. 28 for details)

$$Z_i(i\omega_n) = 1 + \sum_j \lambda_{ij}. \tag{6}$$

This result may now be used in Eq. (1) to obtain

$$\Delta_i(i\omega_n) = \begin{cases} \Delta_i(T), & |\omega_n| < \omega_o \\ 0, & |\omega_n| > \omega_o \end{cases} \tag{7}$$

where

$$\Delta_i(T) = \frac{\pi T}{Z_i} \sum_{m,|\omega_m|<\omega_o} \sum_j \frac{\Delta_j(T)}{\sqrt{\omega_m^2 + \Delta_j^2}} [\lambda_{ij} - \mu_{ij}^*], \tag{8}$$

where ω_o represents either the Debye frequency or some other characteristic energy scale representing the phonons in the system, at most the maximum phonon energy. Detailed justification of using a single cutoff is found in Ref. 11. These results are used to derive various quantities within the $\lambda^{\theta\theta}$ model, which we will call renormalized BCS or RBCS. We also solve the full Eliashberg equations for typical strong coupling parameters and for the case of MgB_2, and in order to connect to the language most appropriate for this purpose, the measure of the characteristic boson frequency, $\omega_{\ln}$, is defined to be

$$\omega_{ln} = \exp\left[\frac{2}{\lambda_{11}} \int_0^\infty \ln(\omega) \frac{\alpha^2 F_{11}(\omega)}{\omega} d\omega \right]. \tag{9}$$

This is reasonable for our case here as the $\omega_{\ln}$ calculated for the different $\alpha_{ij}^2 F(\omega)$ spectra of MgB_2 are almost the same and other spectra used in this paper will have the same frequency distribution in each channel only scaled in magnitude. In general, this definition should be reasonably robust as, unless λ_{22}, λ_{12}, and λ_{21} are large, the first channel λ_{11} should dominate the strong coupling effects.

III. BCS RATIOS: THE $\lambda^{\theta\theta}$ MODEL AND STRONG COUPLING

A. Critical temperature T_c

The critical temperature that results from the renormalized BCS equation (8) of the two-square-well approximation takes the form

$$A = \ln\left(\frac{1.13\hbar\omega_o}{k_B T_c} \right) \tag{10}$$

or

$$k_B T_c = 1.13\hbar\omega_o e^{-A}, \tag{11}$$

where

$$A = \frac{\bar{\lambda}_{11} + \bar{\lambda}_{22} - \sqrt{(\bar{\lambda}_{11} - \bar{\lambda}_{22})^2 + 4\bar{\lambda}_{12}\bar{\lambda}_{21}}}{2(\bar{\lambda}_{11}\bar{\lambda}_{22} - \bar{\lambda}_{12}\bar{\lambda}_{21})} \tag{12}$$

and

$$\bar{\lambda}_{11} = \frac{\lambda_{11} - \mu_{11}^*}{1 + \lambda_{11} + \lambda_{12}}, \quad \bar{\lambda}_{12} = \frac{\lambda_{12} - \mu_{12}^*}{1 + \lambda_{11} + \lambda_{12}},$$

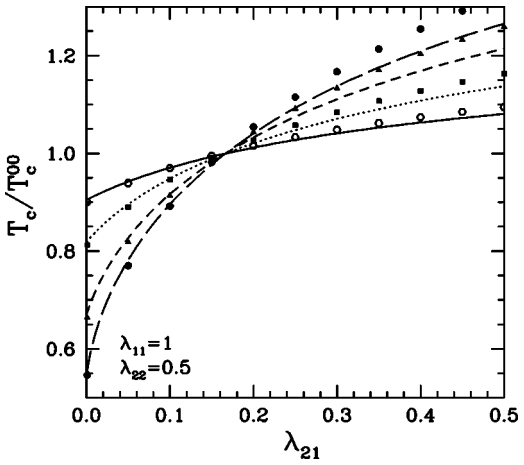

FIG. 1. Ratio of T_c to the pure, one-band T_c^{00} as a function of λ_{21} for varying λ_{12}: 0.6 (long-dashed), 0.4 (short-dashed), 0.2 (dotted), and 0.1 (solid). Here, $\lambda_{11}=1$ and $\lambda_{22}=0.5$. Strong coupling Eliashberg calculations are given for comparison for the same parameters and are shown as the points with λ_{12}: 0.6 (solid circles), 0.4 (solid triangles), 0.2 (solid squares), and 0.1 (open circles).

$$\bar{\lambda}_{22} = \frac{\lambda_{22} - \mu_{22}^*}{1 + \lambda_{22} + \lambda_{21}}, \quad \bar{\lambda}_{21} = \frac{\lambda_{21} - \mu_{21}^*}{1 + \lambda_{22} + \lambda_{21}}. \tag{13}$$

With no impurities and for one band ($\lambda_{12}=\lambda_{21}=\lambda_{22}=0$)

$$k_B T_c^{00} = 1.13\omega_o e^{-1/\bar{\lambda}_{11}}. \tag{14}$$

Here we will be interested only in the ratio of T_c [Eq. (11)] to T_c^{00} [Eq. (14)] and so the cutoff ω_o cancels, and the issue of the best choice for this quantity does not enter (see Allen and Dynes[27]). Results for T_c/T_c^{00} based on Eqs. (11)–(14) as a function of λ_{21} for various values of λ_{12} are shown in Fig. 1, where they are compared with results of complete numerical evaluation of the two-band Eliashberg equations (1) and (2). A Lorentzian model for the spectral densities $\alpha_{ij}^2 F(\omega)$ is used with zero Coulomb pseudopotential μ_{ij}^* for simplicity. Specifically, we use a truncated Lorentzian spectral density, which is defined in Ref. 29, centered around 50 meV with width 5 meV, truncated by 50 meV to either side of the central point. The $\omega_{\ln}$ for this spectrum is 44.6 meV. This spectral density is scaled in each of the four channels to give $\lambda_{11}=1$, $\lambda_{22}=0.5$, and the range of values of λ_{12} and λ_{21} as required for the figure. The curves, which are labeled in the figure caption, are for the renormalized BCS calculations and the corresponding Eliashberg calculations are presented as points. We note that for small values of λ_{21} agreement between the $\lambda^{\theta\theta}$ results and full Eliashberg calculation is excellent. The agreement is somewhat less good around $\lambda_{21}=0.5$ but still acceptable. An interesting point to note about this figure is that the effect on T_c of λ_{21} and λ_{12} are quite different. As λ_{21} increases for fixed λ_{12}, T_c increases. On the other hand, for small but fixed λ_{21}, increasing λ_{12} decreases T_c, while the opposite behavior is found to hold for values of λ_{21} larger than approximately 0.16. This behavior is different from that expected in nonrenormalized BCS theory, where it is known that increasing the off-diagonal coupling from zero to some finite value always increases T_c whatever its sign.

Expanding Eq. (12) under the assumption that the off-diagonal elements are small as compared with the diagonal ones ($\bar{\lambda}_{12}, \bar{\lambda}_{21} \ll \bar{\lambda}_{11} - \bar{\lambda}_{22}, \bar{\lambda}_{22}$) gives

$$A \simeq \frac{1}{\bar{\lambda}_{11}}\left[1 - \frac{\bar{\lambda}_{12}\bar{\lambda}_{21}}{\bar{\lambda}_{22}}\left\{\frac{1}{\bar{\lambda}_{11} - \bar{\lambda}_{22}} - \frac{1}{\bar{\lambda}_{11}}\right\}\right]. \quad (15)$$

In BCS theory, the $\bar{\lambda}_{ij}$ would not be renormalized as in Eq. (13). Since the term in curly brackets is positive, A decreases with the product of $\bar{\lambda}_{12}\bar{\lambda}_{21}$ and hence T_c increases. But in our case, the multiplying term $1/\bar{\lambda}_{11} \equiv (1+\lambda_{11}+\lambda_{12})/\lambda_{11}$ contains λ_{12} in leading order and this factor on its own increases A and therefore decreases the critical temperature. These expectations are confirmed in our full Eliashberg numerical work and are not captured in other BCS works (for example, Refs. 30 and 31). It is clear then, that in our theory, λ_{12} and λ_{21} do not enter the equation for T_c in the same way because λ_{12} provides a direct mass renormalization to the major interaction term λ_{11}. If mass renormalization is ignored, as in BCS theory, this asymmetry no longer arises. The work by Mitrović[32] on functional derivatives finds $\delta T_c / \delta \alpha^2 F_{21}(\omega)$ to be positive and the one for 12 to be negative, which conforms with our results. We note here that the disparity between λ_{12} and λ_{21}, which will in turn affect the T_c and other properties, is related to the different values of the density of states at the Fermi level N_i in each of the two bands, i.e., $\lambda_{12}/\lambda_{21} = N_2/N_1$.

Turning next to the effect of impurities on T_c, the change $\Delta T_c = T_c - T_{c0}$ for small impurity scattering can be written in the $\lambda^{\theta\theta}$ model as

$$\frac{\Delta T_c}{T_{c0}} = \frac{C^{\pm}}{\bar{\lambda}_{11} + \bar{\lambda}_{22} + 2A(\bar{\lambda}_{12}\bar{\lambda}_{21} - \bar{\lambda}_{11}\bar{\lambda}_{22})}, \quad (16)$$

where for ordinary impurities (C^+) and magnetic impurities (C^-):

$$\begin{aligned} C^{\pm} = -\frac{\pi^2}{4}\{&(1 - A\bar{\lambda}_{22})(\rho_{12}^{\pm}\bar{\lambda}_{11} \mp \rho_{21}^{\pm}\bar{\lambda}_{12}) \\ &+ [1 - A\bar{\lambda}_{11}](\rho_{21}^{\pm}\bar{\lambda}_{22} \mp \rho_{12}^{\pm}\bar{\lambda}_{21}) \\ &+ A\bar{\lambda}_{21}(\bar{\lambda}_{12} \mp \bar{\lambda}_{11})\rho_{12}^{\pm} + A\bar{\lambda}_{12}(\bar{\lambda}_{21} \mp \bar{\lambda}_{22})\rho_{21}^{\pm}\}, \end{aligned} \quad (17)$$

with

$$\rho_{12}^{\pm} = \frac{t_{12}^{\pm}/T_{c0}}{1 + \lambda_{11} + \lambda_{12}}, \quad \rho_{21}^{\pm} = \frac{t_{21}^{\pm}/T_{c0}}{1 + \lambda_{22} + \lambda_{21}}. \quad (18)$$

These equations have been derived for scattering across the bands; within the bands, paramagnetic impurities will affect T_c but ordinary, nonmagnetic ones will not.

Results are given in Fig. 2. Except for the dotted lines, all curves were obtained from numerical solutions of the linearized version of the Eliashberg equations (1) and (2) using a Lorentzian model for $\alpha_{ij}^2 F(\omega)$. The curves come in sets of three for $\lambda_{22}=0.5$ (solid curve), 0.4 (dashed), and 0.3 (long-dashed). The other parameters are $\lambda_{11}=1$ and $\lambda_{12}=\lambda_{21}=0.02$ (small interband coupling). The lower set is for $t_{21}^+=0$ with t_{12}^+ varying while the upper set has $1 \leftrightarrow 2$. The middle set have $t_{12}^+ = t_{21}^+$. Note that in showing the results when t_{12}^+ or t_{21}^+ are varied separately, we are violating a requirement that they must be linked together by the density of states in the two bands. That is, as required for the λ_{ij}'s, likewise the impurity scattering rates must obey $t_{12}^+/t_{21}^+ = N_2/N_1$. Our middle set of curves obey this constraint, but we have ignored it for the other curves in order to illustrate the general behavior of each individual type of scattering separately. As found for the λ_{ij}'s, the effect of t_{12}^+ and that of t_{21}^+ on T_c are quite different. The quantity t_{12}^+ represents scattering from band 1 to band 2 and leads to pair breaking much like paramagnetic impurities in the one-band case. We can see this analytically in the simple case of $\lambda_{12}=\lambda_{21}=0$ for which the two bands are decoupled and the critical temperature is a property of the first band alone. In this case, Eqs. (16)–(18) reduce to[33]

$$\frac{\Delta T_c}{T_{c0}} = -\frac{\pi^2}{4}\rho_{12}^{\pm} \quad (19)$$

for both normal or paramagnetic impurities in the linear approximation for the impurity scattering rate. The initial linear decrease in T_c with increasing ρ_{12}^+ is seen in the lower set of three curves of Fig. 2. As t_{12}^+ is increased further, higher-order corrections start to be important and the curves show saturation to a value that is larger the greater the value of λ_{22}. Also note that formula (19) shows that T_c is independent of $\rho_{21}^{\pm}$. This expectation is confirmed in the upper set of three curves of Fig. 2, where T_c has increased by no more than 3% for $t_{21}^+/T_{c0}=1.5$. This small increase is due to the small λ_{12}

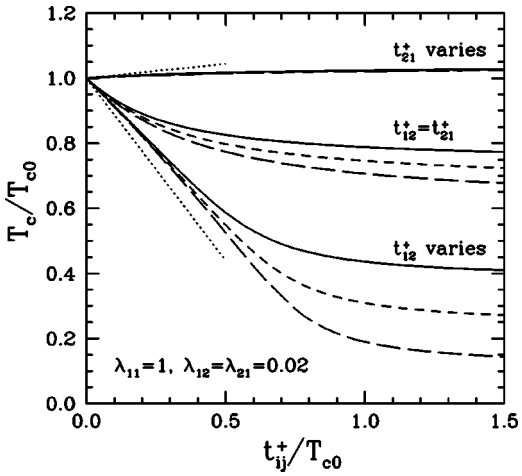

FIG. 2. Ratio of T_c with impurity scattering to that without T_{c0} as a function of t_{ij}^+/T_{c0} for varying λ_{22}: 0.5 (solid), 0.4 (short-dashed), and 0.3 (long-dashed). Here, $\lambda_{11}=1$, $\lambda_{12}=\lambda_{21}=0.02$. For the lower three curves $t_{21}^+=0$ and t_{12}^+ varies, and for the upper three curves (which are almost indistinguishable from each other) it is the reverse. In the middle set of three curves, $t_{12}^+=t_{21}^+$. These calculations have been done with the full Eliashberg equations using a Lorentzian $\alpha^2F(\omega)$ spectrum with $T_{c0}/\omega_{\ln}=0.11$. The dotted lines are from the evaluation of Eq. (16) for the $\lambda_{22}=0.5$ case and are for $t_{12}^+=0$ (upper dotted curve) and $t_{21}^+=0$ (lower dotted curve). (Note that the middle set of curves are the only physically realizable cases. The others serve to make the mathematical point that t_{12}^+ and t_{21}^+ affect T_c quite differently.)

$=\lambda_{21}$ used for the figure, while in Eq. (19) , we have $\lambda_{12}=\lambda_{21}=0$. The middle set of curves, which apply for $t_{12}^{+}=t_{21}^{+}$ and therefore satisfy the constraint imposed by having chosen $\lambda_{12}=\lambda_{21}=0.02$, exhibits, by comparison to the other two cases, only a very small region that is linear in impurity scattering and these curves are intermediate to the other two sets, as expected. They also saturate at higher values of T_c and we find that T_c decreases by only 20–30 % for this case, similar to the observation by Mitrović, who was considering specifically the case of MgB_2.[34] Finally, we comment on the dotted curves, which are based on Eqs. (16)–(18) valid in the $\lambda^{\theta\theta}$ model and to first order in t_{ij}^{+}. The lowest curve applies to the $t_{21}^{+}=0$ case and the upper one to $t_{12}^{+}=0$. The slopes are in good agreement with the full Eliashberg results over a significant range of interband impurity scattering t_{ij}^{+}. For the middle set of curves the linear behavior applies only comparatively to a rather small region. In all cases there is still some difference between $\lambda^{\theta\theta}$ and Eliashberg results because of strong coupling corrections. As previously stated, interband impurity scattering in two-band superconductivity works like paramagnetic impurities in the ordinary one-band case. For this latter case, Schachinger, Daams, and Carbotte[35] have found for the specific case of Pb, the classic strong coupling material, that the $\lambda^{\theta\theta}$ model overestimates the initial slope of the drop in T_c value, with increasing impurity scattering. The physics is simple. For strong coupling, $2\Delta/k_BT_c$ is larger than its BCS value i.e., the gap is bigger than expected on the basis of its T_c. This is because as T is increased, that part of the inelastic scattering which corresponds to the real (as opposed to virtual) processes, which are pair breaking, increases and T_c is reduced below the value it would be without. As a result, the initial drop in the T_c value with increasing impurity content is not as large in strong as in weak coupling because the system has a larger gap that is more robust against impurities. The same applies to interband scattering in a two-band superconductor. The initial slope of the drop is faster in the $\lambda^{\theta\theta}$ model than in the Eliashberg calculation, as most recently shown by Mitrović,[34] who has commented on prior work by Golubov and Mazin,[33] where only unrenormalized BCS results were given and the drop in T_c was even faster. Mitrović also presents functional derivatives for ordinary impurities[34] and his findings compliment our calculations here. In addition, as low-frequency phonons act like ordinary impurities, the previous work by Mitrović on functional derivatives[32] for the electron-phonon spectral functions also confirms our impurity results by comparison with the behavior of the low-frequency part of the functional derivatives for 12 versus 21.

Finally, it has been of some interest among experimentalists, looking at novel superconductors, to know the outcome of having a repulsive interaction in the second band (i.e., $\lambda_{22}<0$). As will be seen in the next section, a second energy gap is still induced in this case due to the interband coupling; however, a signature of this repulsive band would exist in the case of impurity scattering, as strong interband scattering of sufficient strength could drive the T_c to zero.[30]

B. Energy gaps and gap ratios

We turn next to the consideration of the energy gaps. The transcendental equation for $u\equiv\Delta_2/\Delta_1$ at $T=0$ in the $\lambda^{\theta\theta}$ model is

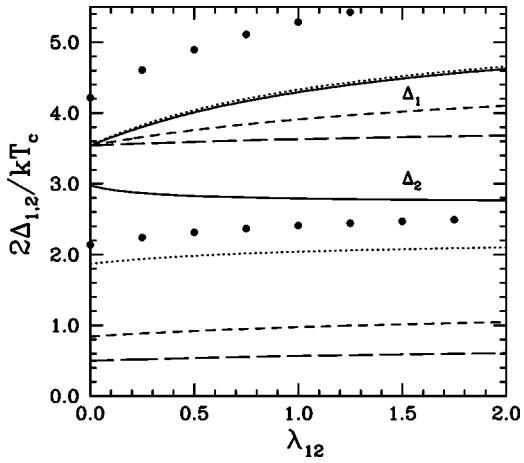

FIG. 3. Gap ratios for the upper $(2\Delta_1/k_BT_c)$ and lower gap $(2\Delta_2/k_BT_c)$ as a function of λ_{12} for varying λ_{22}: 0.5 (solid), 0.1 (dotted), −0.5 (short-dashed), and −1 (long-dashed). Here, $\lambda_{11}=1$, $\lambda_{21}=0.3$. These calculations are done using the RBCS formulas (20) and (21) in the text, the solid dots show Eliashberg calculations for the same set of parameters with $\lambda_{22}=0.1$ (for comparison with the dotted curve). Strong coupling corrections are significant and the rest of the curves in this figure would also be modified by strong coupling; much of this can be captured by the strong coupling correction formula given in the text. (Note that as λ_{22} and λ_{21} are finite, the points for $\lambda_{12}=0$ are not physically realizable.)

$$\bar{\lambda}_{12}u-\frac{\bar{\lambda}_{21}}{u}+(\bar{\lambda}_{11}\bar{\lambda}_{22}-\bar{\lambda}_{21}\bar{\lambda}_{12})\ln u=\bar{\lambda}_{22}-\bar{\lambda}_{11}, \quad (20)$$

from which the gap ratio for the larger gap Δ_1 may be found:

$$\ln\left(\frac{1.13\Delta_1}{2k_BT_c}\right)=A-\left[\frac{1+\bar{\lambda}_{12}u\ln u}{\bar{\lambda}_{11}+\bar{\lambda}_{12}u}\right]. \quad (21)$$

The solution for the gap ratio $2\Delta_1/k_BT_c$ can be corrected for strong coupling effects by multiplying by a factor η_Δ in the denominator of the logarithm of Eq. (21) with[36]

$$\eta_\Delta=1+12.5\left(\frac{T_c}{\omega_{\ln}}\right)^2\ln\left(\frac{\omega_{\ln}}{2T_c}\right). \quad (22)$$

As long as λ_{11} is large and λ_{22}, λ_{12}, and λ_{21} are small, one needs only to correct the first channel for strong coupling effects. Otherwise additional corrections for the other channels may exist but there would be no merit in such a complexity of including these corrections over doing the full numerical calculations with the Eliashberg equations. It is expected that in real systems, λ_{11} is large relative to the other parameters and hence dominates the strong coupling aspect of the result. However, when the off-diagonal couplings are significant, the strong coupling corrections of the first channel can affect the second.

Our first set of results for the two energy gaps is given in Fig. 3. The lines are based on the simpler equations (20) and (21), and the solid dots are for the results of full Eliashberg solutions on the imaginary axis and analytically continued with Padé approximates[1] to the real axis, where the gap is determined by $\Delta_0=\Delta(\omega=\Delta_0)$.[1] For clarity in the figure, only

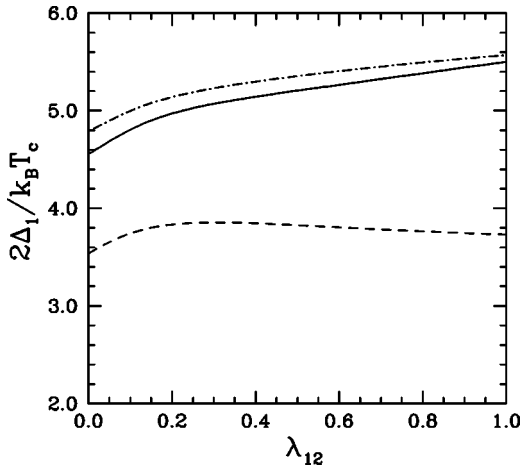

FIG. 4. Gap ratio $2\Delta_1/k_BT_c$ as a function of $\lambda_{12}=\lambda_{21}$, for $\lambda_{11}=1.3$ and $\lambda_{22}=0.5$. These curves provide a comparison between the Eliashberg calculation (solid curve) and the RBCS calculation (dashed curve), along with the result from using the RBCS expression with the strong coupling correction formula given in the text (dot-dashed curve).

one such set of results is shown for the case of $\lambda_{22}=0.1$. While magnitudes differ considerably between the renormalized BCS and strong coupling (comparing solid dots with the dotted curves), the general trends are the same. Specifically in Fig. 3, λ_{12} is varied with $\lambda_{11}=1$, $\lambda_{21}=0.3$, and λ_{22} fixed to various values in turn. The upper curve applies to Δ_1 and the lower curve of the same line type to Δ_2. While in all cases Δ_1 increases with increasing λ_{12}, in one case (solid curve), the lower gap decreases slightly. More importantly, the value of the upper gap ratio increases above its BCS ratio 3.53 and can reach 4.6 in renormalized BCS, a feature that comes from the two-band nature of the system. Comparing the dotted curves to the solid circles for Δ_1, we note that the Eliashberg results are always above their $\lambda^{\theta\theta}$ counterpart, reflecting well-known strong coupling corrections to the gap. This applies as well to Δ_2, the lower gap. We now comment specifically on the other curves. To increase the anisotropy between Δ_1 and Δ_2 for the parameter set considered here, we need to decrease the value of λ_{22}. Note, however, that even when we assume a repulsion in the second band, equal in size to the attraction $\lambda_{11}=1$ in the first band (long-dashed curve), a substantial gap is nevertheless induced in the second channel even for $\lambda_{12}=0$. It is the finite value of λ_{21} that produces this gap. Recall that λ_{21} describes the effect of band 1 on band 2 due to interband electron-phonon coupling. Turning on, as well, some λ_{12} increases the second gap further but not by much. Finally, we mention that as λ_{21} increases (not shown here), Δ_1 decreases while Δ_2 increases, i.e., the ratio of Δ_2/Δ_1 goes up towards one and the anisotropy is reduced.

In Fig. 3, the ratio $\lambda_{12}/\lambda_{21}=N_2/N_1$ is varying, while in Fig. 4, we keep $\lambda_{12}=\lambda_{21}$ and illustrate more clearly the effect of strong coupling Eliashberg results in comparison with the RBCS calculation, and also provide a comparison with the RBCS calculation corrected with the strong coupling formula of Eq. (22) . One finds that the gap in the Eliashberg result is quite enhanced over the RBCS result, even exhibiting a different qualitative behavior with the Eliashberg gap (solid curve), increasing with increasing off-diagonal λ while the RBCS counterpart (dashed curve) is decreasing. However, when the strong coupling correction formula is applied to the RBCS result, the resulting curve (dot-dashed) is now in reasonable agreement with the Eliashberg calculation and follows the evolution with increasing off-diagonal λ very well.

It is of interest to experimentalists,[37] looking at novel materials suspected of harboring multiband superconductivity, whether there may be a range of parameters that could produce a very large upper gap ratio with a large anisotropy in magnitude between the upper and lower gaps. It is possible that it could occur in a regime where $\lambda_{12}/\lambda_{21}\gg 1$, as suggested by the trend in our Fig. 3, while in the opposite regime we will show that all results return to standard weak coupling BCS values. As previously mentioned, this ratio of $\lambda_{12}/\lambda_{21}$ is equivalent to the ratio of density of states in the two bands, sometimes denoted as α in the literature, i.e., $\alpha \equiv \lambda_{12}/\lambda_{21}=N_2/N_1$. We have gone to $\alpha=20$ within the renormalized BCS formalism and were not able to produce gap ratios bigger than about 5 or so, for the parameters examined, and at the same time, the lower gap ratio was about 3. We conclude, therefore, that even with added strong coupling effects, very large gap ratios tending towards 10 to 20 are difficult to obtain in conjunction with a large anisotropy in the two gaps. Repulsive potentials in the second band can give a large anisotropy, but they also lower the value of the upper gap ratio. Later in Sec. VI, we will return to this issue of trying to obtain large gap ratios and large gap anisotropy, when we examine another extreme limit first considered by Suhl *et al.*[9]

To conclude this section, we examine an approximate formula for the gap ratio in two-band superconductivity, which has been given and used by experimentalists,[38] to determine its range of validity in the face of more exact calculations. The formula is an unrenormalized BCS formula and we have already seen that renormalization and strong coupling effects can be substantial. For $\lambda_{22},\lambda_{12},\lambda_{21}\ll\lambda_{11}$, we can derive the primary (or large) gap ratio as

$$\frac{2\Delta_1}{k_BT_c}\simeq 3.53\left[1-\frac{\lambda_{12}}{\lambda_{21}}u^2\ln u\right]=3.53\left[1-\frac{N_2}{N_1}\left(\frac{\Delta_2}{\Delta_1}\right)^2\ln\left(\frac{\Delta_2}{\Delta_1}\right)\right], \tag{23}$$

which is the same equation as given by Iavarone *et al.*,[38] where their use of the indices 1 and 2 are reversed with respect to ours. In our formula (23) given here, the u and λ's are coupled through Eq. (20) , but in the case of Ref. 38 the ratio of the density of states and the ratio of the gaps are treated as independent parameters with the only constraint being that $u\ll 1$.

In Fig. 5, we compare this approximate BCS formula with that of our exact renormalized BCS formula for typical λ_{ij} values used in the literature. The μ_{ij}^* are set to zero as there is no such feature in the Iavarone *et al.* formula and the μ^*'s in that case would simply serve to change the effective value of λ's. We find that the approximate formula (dashed curve of Fig. 5) compares well with the renormalized BCS result in the limit of small $\lambda_{12,21,22}$, as required by the constraint of the approximation, and breaks down for $\lambda_{12}>0.5$, where the ap-

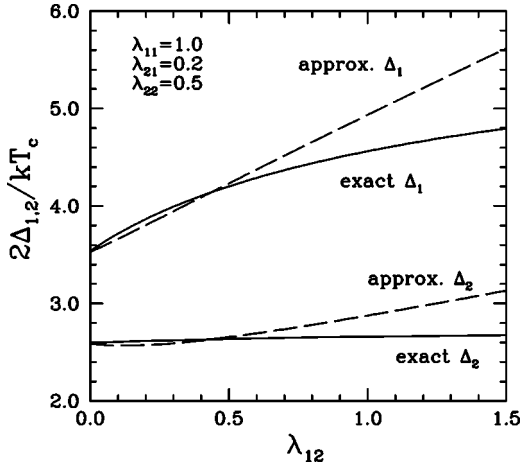

FIG. 5. Gap ratios for the upper $(2\Delta_1/k_BT_c)$ and lower gap $(2\Delta_2/k_BT_c)$ as a function of λ_{12} for $\lambda_{11}=1.0$, $\lambda_{22}=0.5$, $\lambda_{21}=0.2$. The solid curve is the exact BCS result, whereas the dashed curve illustrates the approximate formula of Iavarone *et al.* (Ref. 38).

proximate formula tends to overestimate quite significantly the value of the two gaps. Strong coupling effects would produce very significant deviations in addition. Not shown is the case where $\lambda_{12,21,22}$ were all taken to be very small and then in that case, as expected, there was excellent agreement between the exact renormalized BCS calculation and the approximate form. The fact that Iavarone *et al.*[38] obtained excellent estimates of the two energy gaps for MgB_2 is maybe fortuitous in some sense, because it will be seen in the next section, where we discuss MgB_2 in detail, that the renormalized BCS formula underestimates the correct gap values of MgB_2 and strong coupling corrections of about 7–10 % are needed to obtain good agreement between the data and full Eliashberg calculations. We conclude that their simple formula is helpful, but that it should be used with caution when considering systems where the parameters are no longer small as then this formula will fail.

C. Specific heat jump

The specific heat is calculated from the free energy. The difference in free energy $\Delta F=F_S-F_N$ between the superconducting state and the normal state is given by[1]

$$\Delta F = -\pi T \sum_{n=-\infty}^{+\infty} \sum_i N_i(0)[\sqrt{\omega_n^2+\Delta_i^2(i\omega_n)}-|\omega_n|] \times \left[Z_i^S(i\omega_n) - Z_i^N(i\omega_n)\frac{|\omega_n|}{\sqrt{\omega_n^2+\Delta_i^2(i\omega_n)}}\right], \quad (24)$$

where S and N refer to the superconducting and normal state, respectively, and i indexes the number of bands. From this, the difference in the specific heat is obtained,

$$\Delta C = -T\frac{d^2\Delta F}{dT^2}, \quad (25)$$

and the negative of the slope of the difference in specific heat near T_c is given as

$$g = -\left.\frac{d\Delta C(T)}{dT}\right|_{T_c}\frac{1}{\gamma}, \quad (26)$$

where γ is the Sommerfeld constant for the two-band case.

In the $\lambda^{\theta\theta}$ model, the gap near T_c, for $t=T/T_c$, can be written as

$$\Delta_1^2(t) = \frac{8(\pi T_c)^2}{7\zeta(3)}\frac{\eta_C}{\chi_1}(1-t), \quad (27)$$

$$\Delta_2^2(t) = \frac{8(\pi T_c)^2}{7\zeta(3)}\frac{1}{\chi_2}(1-t), \quad (28)$$

where $\zeta(3)\simeq 1.202$. Here,

$$\chi_1 = \frac{(1-A\overline{\lambda_{22}})\overline{\lambda_{11}}+\overline{\lambda_{12}}\overline{\lambda_{21}}A[1+A^2\overline{\lambda_{21}^2}(1-A\overline{\lambda_{22}})^{-3}]}{(1-A\overline{\lambda_{22}})\overline{\lambda_{11}}+\overline{\lambda_{12}}\overline{\lambda_{21}}[2A+A^2\overline{\lambda_{22}}/(1-A\overline{\lambda_{22}})]} \quad (29)$$

and

$$\chi_2 = \frac{(1-A\overline{\lambda_{11}})\overline{\lambda_{22}}+\overline{\lambda_{21}}\overline{\lambda_{12}}A[1+A^2\overline{\lambda_{12}^2}(1-A\overline{\lambda_{11}})^{-3}]}{(1-A\overline{\lambda_{11}})\overline{\lambda_{22}}+\overline{\lambda_{21}}\overline{\lambda_{12}}[2A+A^2\overline{\lambda_{11}}/(1-A\overline{\lambda_{11}})]}, \quad (30)$$

and the strong coupling correction is introduced through[39]

$$\eta_C = 1+53\left(\frac{T_c}{\omega_{\ln}}\right)^2\ln\left(\frac{\omega_{\ln}}{3T_c}\right). \quad (31)$$

The specific heat jump at T_c is

$$\frac{\Delta C}{\gamma T_c} = 1.43\left[\frac{(1+\lambda_{11}+\lambda_{12})(\eta_C/\chi_1)+\alpha(1+\lambda_{22}+\lambda_{21})(1/\chi_2)}{(1+\lambda_{11}+\lambda_{12})+\alpha(1+\lambda_{22}+\lambda_{21})}\right]. \quad (32)$$

We find with this expression that anisotropy (i.e., $\lambda_{11}\neq\lambda_{22}$) reduces the jump ratio but increasing λ_{12} or λ_{21} increases the ratio, and the maximum obtainable is 1.43. Other work along the same line is given in Refs. 30 and 31 where they do not consider full renormalized BCS or strong coupling theories, as we have done here.

When $\lambda_{12},\lambda_{21}\to 0$, $1/\chi_1\sim 1+O(\overline{\lambda_{12}^2})$ and $1/\chi_2\sim O(\overline{\lambda_{12}^4})$. This is assuming $\overline{\lambda_{11}}-\overline{\lambda_{22}}$ and $\overline{\lambda_{22}}$ remain significant as compared with the value of the off-diagonal elements. In this case,

$$\frac{\Delta C}{\gamma T_c} = 1.43\left[\frac{(1+\lambda_{11}+\lambda_{12})}{(1+\lambda_{11}+\lambda_{12})+\alpha(1+\lambda_{22}+\lambda_{21})}\right]. \quad (33)$$

The physics of this formula is that, in this limit, the specific heat jump at T_c itself is determined only by the superconductivity of the dominant band, but it is normalized with the normal state specific heat γ belonging to the sum of both bands. This has the effect of making $\Delta C(T_c)/\gamma T_c$ always less than the BCS value by a factor of $1/(1+\alpha^*)$, where $\alpha^*=\alpha(1+\lambda_{22}+\lambda_{21})/(1+\lambda_{11}+\lambda_{12})$. For MgB_2, we expect α^*

$\gtrsim 1$, which means that in this case the normalized jump is reduced to about half its BCS value. If we had included in Eq. (33) the strong coupling correction η_C, this would have the effect of increasing the factor 1.43 to a larger value characteristic of strong coupling but the additional anisotropy parameters would still work to reduce the jump. Thus, in a two-band superconductor, the jump will be smaller than that for one band with the same strong coupling index

D. Thermodynamic critical magnetic field

The thermodynamic critical magnetic field is calculated from the free energy difference:

$$H_c(T) = \sqrt{-8\pi\Delta F}. \tag{34}$$

As the temperature dependence of this quantity, normalized to its zero-temperature value, follows very closely a nearly quadratic behavior, the deviation function $D(t)$ is often plotted:

$$D(t) \equiv \frac{H_c(T)}{H_c(0)} - (1 - t^2), \tag{35}$$

where $t = T/T_c$.

At $T=0$

$$H_c^2(0) = 4\pi N_1^* \Delta_1^2 (1 + \alpha^* u^2), \tag{36}$$

where $\alpha^* = N_2^*/N_1^*$ and

$$N_i^* = N_i(0)(1 + \lambda_{ii} + \lambda_{ij}). \tag{37}$$

The zero-temperature critical magnetic field is modified through the second term in Eq. (36) , which increases with increasing α^* and with the square of the anisotropy ratio u, which in this case is just the ratio of the independent gap values for the two separate bands. Further, the dimensionless ratio is

$$\frac{\gamma T_c^2}{H_c^2(0)} = \frac{\pi (k_B T_c)^2 [1 + \alpha^*]}{6\Delta_1^2 [1 + \alpha^* u^2]}. \tag{38}$$

For almost decoupled bands, Eq. (38) becomes

$$\frac{\gamma T_c^2}{H_c^2(0)} = 0.168 \frac{1 + \alpha^*}{1 + \alpha^* u^2}, \tag{39}$$

where the second factor on the right-hand side modifies the usual single-band BCS value of 0.168 for the presence of the second band. Again, both α^* and u enter the correction. If there is no anisotropy, $u=1$, and therefore the bands must be the same, we recover the one-band limiting value. For large anisotropy where $u \to 0$, and if α^* is of order one, the ratio in Eq. (39) is of order twice its one-band value because the second band contributes very little to the zero-temperature condensation energy, but is still as equally important as the first band in its contribution to γT_c, the normal state specific heat. Near T_c

$$H_c(t) = \sqrt{\frac{32\pi}{7\zeta(3)}} (\pi k_B T_c)(1 - t) \left[\frac{N_1^*}{\chi_1^2} + \frac{N_2^*}{\chi_2^2} \right]^{1/2}, \tag{40}$$

which then gives the dimensionless ratio

$$h_c(0) \equiv \frac{H_c(0)}{|H_c'(T_c)| T_c} = \frac{2\Delta_1}{k_B T_c} \frac{1}{\pi} \sqrt{\frac{7\zeta(3)}{32}} \sqrt{\frac{1 + \alpha^* u^2}{\chi_1^{-2} + \alpha^* \chi_2^{-2}}}. \tag{41}$$

Strong coupling factors could be introduced in Eqs. (36), (38), and (40). They are not given explicitly here as they are less important than those for the specific heat jump and the slope of the penetration depth at T_c (see Table I). The limit of nearly decoupled bands ($\overline{\lambda}_{12}, \overline{\lambda}_{21} \ll \overline{\lambda}_{11} - \overline{\lambda}_{22}, \overline{\lambda}_{22}$) gives for this quantity

$$h_c(0) = 0.576 \sqrt{1 + \alpha^* u^2}. \tag{42}$$

The square root, which accounts for two-band effects contains a correction proportional to $\alpha^* u^2$. It can be understood as follows. The slope at T_c found from formula (40) depends only on band 1 but $H_c(0)$ involves both and hence this correction comes solely from $H_c(0)$ as seen in Eq. (36) . If the anisotropy between the two bands is large $u \to 0$, there is no correction factor in (42) because the second band is eliminated from $H_c(0)$. If, on the other hand, u is near 1, the two bands have nearly equal gap value but still it is only band 1 which contributes to the slope at T_c and the dimensionless ratio (42) can now be larger than its BCS value.

E. Penetration depth

The London penetration depth $\lambda_L(T)$ is evaluated from[1]

$$\frac{1}{\lambda_L^2(T)} = \frac{T}{2} \sum_{n=1}^{\infty} \sum_i \frac{1}{\lambda_{ooi}^2} \frac{\Delta_i^2(i\omega_n)}{Z_i(i\omega_n)[\omega_n^2 + \Delta_i^2(i\omega_n)]^{3/2}}, \tag{43}$$

where in three dimensions

$$\frac{1}{\lambda_{ooi}^2} = \frac{4\pi n_i e^2}{m_i c^2} = \frac{8\pi e^2}{3c^2} N_i v_{Fi}^2 \tag{44}$$

and v_{Fi} is the Fermi velocity in the band labeled by the index i. This last equation would be multiplied by a factor of 3/2 in two dimensions.

For the penetration depth $\lambda_L(T)$ at $T=0$,

$$\frac{1}{\lambda_L^2(0)} = \frac{1}{\eta_{\lambda_L}^2(0) \lambda_{oo1}^2 (1 + \lambda_{11} + \lambda_{12})} + \frac{1}{\lambda_{oo2}^2 (1 + \lambda_{22} + \lambda_{21})}, \tag{45}$$

and near T_c,

$$\frac{1}{\lambda_L^2(t)} = 2(1 - t) \left[\frac{1}{\eta_{\lambda_L}^2(T_c) \lambda_{oo1}^2 \chi_1 (1 + \lambda_{11} + \lambda_{12})} + \frac{1}{\lambda_{oo2}^2 \chi_2 (1 + \lambda_{22} + \lambda_{21})} \right], \tag{46}$$

where

$$\eta_{\lambda_L}(0) = 1 + 1.3 \left(\frac{T_c}{\omega_{ln}} \right)^2 \ln \left(\frac{\omega_{\ln}}{13 T_c} \right), \tag{47}$$

TABLE I. Universal dimensionless BCS ratios and their modification for strong coupling (SC) and two-band superconductivity. RBCS stands for the renormalized BCS formula given in text. The percentage difference between the full Eliashberg (Eliash.) calculation and RBCS, used to measure the amount of strong coupling correction, is given as % SC and defined as $|(\text{Eliash.}-\text{RBCS})/\text{Eliash.}|$.

Ratio	BCS One band	Pb One band	MgB_2 Eliash.	MgB_2 Expt.	MgB_2 RBCS	MgB_2 % SC	MgB_2 RBCS+SC	Lor. Eliash.	Lor. RBCS	Lor. % SC	Lor. RBCS+SC
T_c/ω_{ln}	0.0	0.128	0.051	0.076[a]	0.0		0.052	0.15	0.0		0.15
$2\Delta_1/k_BT_c$	3.53	4.49	4.17	3.6–4.6[b]	3.86	7.4%	4.15	4.97	3.84	23%	5.14
$2\Delta_2/k_BT_c$	3.53	4.49	1.55	1.0–1.9[b]	1.40	9.7%		2.66	2.27	15%	
Δ_2/Δ_1	1.00	1.00	0.37	0.30–0.42[b]	0.36	2.7%		0.535	0.593	11%	
$\Delta C/\gamma T_c$	1.43	2.79	1.04	0.82–1.32[c]	0.817	21%	1.02	2.08	1.07	49%	1.97
g	−3.77	−12.68	−3.28	−(2.37–4.31)[d]				−8.32			
$\gamma T_c^2/H_c^2(0)$	0.168	0.132	0.225	0.183[e]	0.247	9.8%		0.153	0.193	26%	
$h_c(0)$	0.576	0.465	0.581	0.518–0.667[f]	0.629	8.3%		0.500	0.621	24%	
y	0.5	0.311	1.25	1.22,[g] 0.547[h]	1.50	20%	1.32	0.536	0.861	61%	0.569

[a]Reference 25.
[b]References 38 and 44–49.
[c]References 25, 40, 48, and 50.
[d]Estimated from References 25, 40, and 48.
[e]Reference 40.
[f]Estimated from Refs. 25, 40, and 51.
[g]Estimated from data of Ref. 41 as presented in Ref. 17.
[h]Estimated from Ref. 42.

$$\eta_{\lambda_L}(T_c) = 1 - 16\left(\frac{T_c}{\omega_{ln}}\right)^2 \ln\left(\frac{\omega_{\ln}}{3.5T_c}\right). \tag{48}$$

Hence, defining $y_L(T)=1/\lambda_L^2(T)$, we write the dimensionless BCS penetration depth ratio y as

$$y \equiv \frac{y_L(0)}{|y_L'(T_c)|T_c} = \frac{1}{2}(1+\alpha\beta)\left[\frac{1}{\chi_1}+\frac{\alpha\beta}{\chi_2}\right]^{-1}, \tag{49}$$

where $\beta=v_{F2}^2(1+\lambda_{11}+\lambda_{12})/v_{F1}^2(1+\lambda_{22}+\lambda_{21})$. β is expected to be of order 1 unless there is a great disparity in the two Fermi velocities. For MgB_2, we use the values of $v_{F1}=4.40\times10^5$ m/s and $v_{F2}=5.35\times10^5$ m/s reported in Ref. 18 and for our other model calculations, we take them to be equivalent, for simplicity. For the nearly decoupled case

$$\frac{y_L(0)}{|y_L'(T_c)|T_c} = \frac{1}{2}(1+\alpha\beta). \tag{50}$$

For α and β equal to one, we see that the normalized slope of the penetration depth is twice its one-band BCS value of $1/2$. Should α, β, or both be much larger than 1, then the slope can be even larger, which reflects the fact that only the dominant band determines the slope y_L' but both bands contribute to $y_L(0)$. Information on v_{Fi} and $N_i(0)$ is contained in the slope.

IV. MgB_2: INTEGRATED BANDS AND STRONG COUPLING

We now continue beyond renormalized BCS formulas to evaluate quantities based on the full two-band Eliashberg formalism and we begin with the specific case of MgB_2 and strong coupling effects. Equations (1) and (2) were solved for electron-phonon spectral densities $\alpha_{ij}^2F(\omega)$, read from graphs in Ref. 32, which were originally presented in Ref. 19. The Coulomb repulsion parameters μ_{ij}^* and λ_{ij}, taken from Ref. 19, were $\lambda_{\sigma\sigma}=1.017$, $\lambda_{\pi\pi}=0.448$, $\lambda_{\sigma\pi}=0.213$, $\lambda_{\pi\sigma}=0.155$, $\mu_{\sigma\sigma}^*=0.210$, $\mu_{\pi\pi}^*=0.172$, $\mu_{\sigma\pi}^*=0.095$, and $\mu_{\pi\sigma}^*=0.069$, with $\omega_c=750$ meV. From these parameters, T_c was found to be 39.5 K. As discussed in our theory introduction, we used $\omega_{\ln}=66.4$ meV, calculated from the $\alpha_{11}^2F(\omega)$ spectrum, to form our strong coupling index $T_c/\omega_{\ln}$. The other three channels had $\omega_{\ln}\simeq62$ meV, which is not so different, although as argued previously, the main strong coupling effects will come from the 11 channel, and hence the choice of 66.4 meV for this parameter. From the solution of the Eliashberg equations, we can evaluate Eq. (24) for the free energy difference between the superconducting and normal state, and evaluate the superfluid density or the inverse square of the penetration depth from Eq. (43) . In Fig. 6, which has three frames [the top is the specific heat, middle, the penetration depth, and bottom, the critical magnetic field deviation function of formula (35)], we compare Eliashberg results (solid curve) with experimental results (solid and open circles, triangles, and squares).

In all cases, the agreement with experiment is very good and certainly as good as obtained in conventional one-band cases.[1] In each case, we also present a second set of theoretical results (dashed curve) for which all microscopic parameters remain those of MgB_2 except that we have half the value of the off-diagonal spectral functions $\alpha_{12}^2F(\omega)$ and $\alpha_{21}^2F(\omega)$, which changes the T_c only by about 1 K. It is clear that doing this reduces greatly the quality of the fit one obtains with the experimental data. This can be taken as evidence that the electronic structure, first-principle calculations of electron-phonon spectral functions are accurate. It also

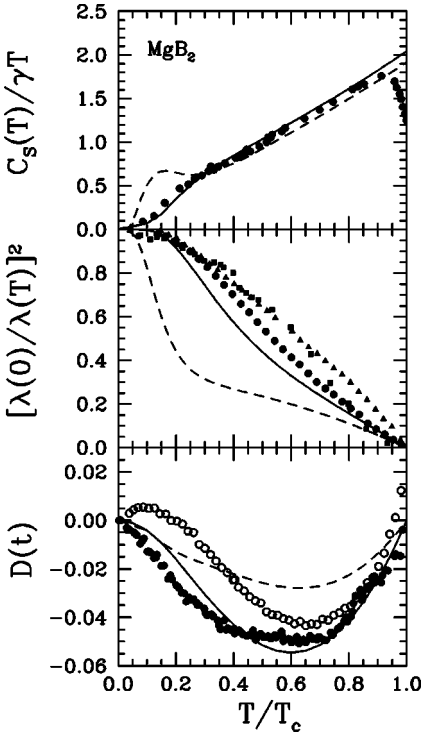

FIG. 6. Upper frame: Electronic specific heat for MgB_2 in the superconducting state normalized to the normal state as a function of T/T_c. The points are the experimental results of Wang *et al.* (Ref. 25) and the solid curve is the result for the Eliashberg calculation using the parameters given in the literature (Ref. 32). The dashed curve illustrates the case where the λ_{12} and λ_{21} parameters, used for the solid curve, have been halved. The jump due to the lower gap begins to appear in this case. Middle frame: $[\lambda(0)/\lambda(T)]^2$ vs T/T_c. Curves are those resulting from the same set of parameters as discussed for the upper frame, with the v_{Fi} taken from Ref. 18. The data, shown for comparison, have been taken from Ref. 17. No impurity scattering has been used to obtain a better fit. Lower frame: The deviation function $D(t)$ for the thermodynamic critical field. Line labels are as above and the data (open and solid circles) are formed from the $H_c(T)$ data given by Wang *et al.* (Ref. 25) and Bouquet *et al.* (Ref. 40), respectively.

shows that variation of parameters by a factor of 2 or so away from the computed ones can lead to significant changes in superconducting properties, and, in this instance, features of the second transition, due to the lower gap, begin to appear. The specific heat curve was computed before in Refs. 15 and 16 and the penetration depth in Refs. 17 and 26. In these cases, our calculations (solid curves) confirm previous ones and demonstrate that our calculational procedure is working correctly. For the penetration depth we did not introduce impurity scattering. Impurities can affect the penetration depth and were included in Ref. 17. The three sets of penetration depth data are for clean (solid circles[41] and triangles[42]) and dirty samples (solid squares[43]) as discussed in Ref. 17. To our knowledge, the deviation function has not been computed and compared with experiment before. The data are from Refs. 25 (open circles) and Ref. 40 (solid circles), and again agreement with calculation, with no free parameters, is very good. The minimum in the deviation

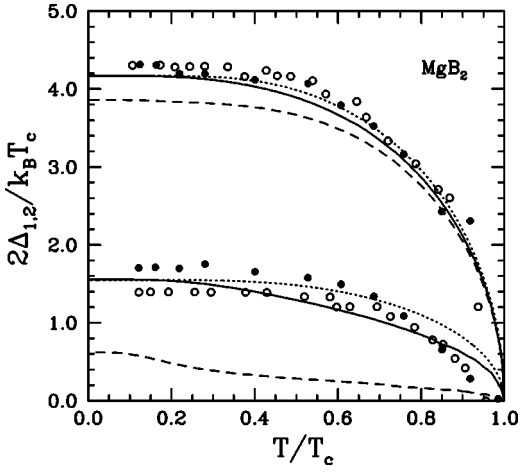

FIG. 7. Gap ratios for the upper $(2\Delta_1/k_BT_c)$ and lower gap $(2\Delta_2/k_BT_c)$ as a function of T/T_c. Shown as the solid curves are the predictions for the gap ratios given by our full Eliashberg calculations for MgB_2, the dashed curves are the Eliashberg calculations for the case of reducing the off-diagonal λ's by half and the dotted curves show the classic BCS temperature dependences to illustrate the deviation of the temperature dependence of the Eliashberg two-band calculation for MgB_2. The open circles are the data from Iavarone *et al.* (Ref. 38), where we have used $T_c=38.3$ K to obtain their quoted upper gap ratio value of 4.3. The solid dots are the data of Gonnelli *et al.* (Ref. 44).

function for the Eliashberg calculation occurs at $T/T_c=0.6$ and has a value of -0.054. In the experimental data, the minima occur at about $T/T_c=0.6$ and 0.65, with values of about -0.05 and -0.045, respectively. For reference, the one-band BCS value is -0.037 and strong coupling makes this value even smaller and can even push it to a positive value; hence anisotropy is compensating for the strong coupling effects and is making this value larger and more negative.[1]

In Fig. 7, we present the temperature dependence of the two gap ratios for MgB_2. Once again the solid curve is the full Eliashberg calculation using the parameters given for MgB_2 with no adjustments. The ratio Δ_1/Δ_2 increases from 2.7 at $T=0$ to about 3.5 at T_c. The temperature-dependent behavior shown here was also found by Choi *et al.*,[16] Brinkman *et al.*,[18] and Golubov *et al.*[19] A comparison with some of the more recent experiments is given by the open and closed circles, with the data taken from Iavarone *et al.*[38] and Gonnelli *et al.*,[44] respectively. Similar data are found in other references.[45–47] In the case of the data by Iavarone *et al.*, the statement of T_c was ambiguous and so we used their quoted value of the upper gap ratio of 4.3 along with their quoted value of the upper gap being 7.1 meV to determine $T_c=38.3$ K used for the scaling of the data for the plot presented here. The Gonnelli *et al.* data are presented based on the T_c of 38.2 K given in their paper. There is a very reasonable agreement of the data with the calculation; once again, along with Fig. 6, this shows a consistency of a number of sets of data from several different types of experiments with the one set of parameters fixed from band structure for MgB_2. Thus overall, the agreement between theory and experiment is excellent and validates the two-band nature of superconductivity in this material. The dotted curves in Fig.

7 are presented to show that the two-band calculations do show deviation from a classic BCS temperature dependence (which was used in the original presentations of the data[38,44]). In particular, Gonnelli *et al.* argued that the deviation of their lower gap data at temperatures above 25 K (or $T/T_c=0.65$, here) from the BCS temperature dependence is an additional signature of the two-band nature of the material. However, we find no such dramatic suppression in the two-band calculations at this temperature and only with the dashed curve, where we have taken the off-diagonal electron-phonon coupling to be half of the usual value for MgB_2 do we find an inflection point around 0.35. We were not able to induce a suppression of the lower gap in the vicinity of T_c by varying the MgB_2 parameters slightly about their accepted values. However, such behavior can be found in other regimes of the parameter space not relevant to MgB_2, and this feature and the issue raised by Gonnelli *et al.* will be discussed further in the next section. To end, note that an inflection point is also seen in the penetration depth at about $T/T_c\sim 0.35$, as described first by Golubov *et al.*[17] and also found here (solid curve of middle frame of Fig. 6).

More results from our calculations as well as comparison with data are presented in Table I. In the first column, we include, for comparison, the one-band BCS values for the various dimensionless ratios. The strong coupling index is first, followed by the major gap to critical temperature ratio, the minor gap ratio, the anisotropy Δ_2/Δ_1, the normalized specific heat jump and the negative of its slope at T_c, $\gamma T_c^2/H_c^2(0)$, and the inverse of the normalized slope at T_c for the critical magnetic field and for the penetration depth. Included in the second column, also for comparison, are the same indices for Pb, the prototype single-band strong coupler. We remind the reader that in many conventional superconductors, strong coupling corrections are large and that the data cannot be understood without introducing them, and these are to be differentiated from those corrections due to anisotropy. The third column gives the results of our two-band calculations for MgB_2. This is followed by a column giving experimental values. It is clear that the agreement between theory and experiment is good. Note that we have not attempted to make a complete survey of all experiments, but have tried to present as many as reasonable, with no judgement about the quality of the data or samples, which might have improved over time. In addition, for the quantities related to slopes, i.e., g, $h_c(0)$, and y, we have tried to estimate these ourselves from the graphs in papers and so this should be viewed as rough estimates as the values might change with a more rigorous analysis of the original data. Also shown are the results when our renormalized BCS formulas of the preceding section are implemented using MgB_2 parameters,[52] which allows us to define a measure of strong coupling corrections, entered in column 6 as percentages. It is seen that MgB_2 is an intermediate coupling case. The next column shows the results when the analytical expressions for strong coupling corrections to renormalized BCS, given in the text, are applied. This improves the agreement with the full Eliashberg results as compared to RBCS. Some discrepancies remain due in part to additional modifications introduced by the coupling of a strong coupling band with a weak coupling one through the off-diagonal λ_{ij}'s. The next four

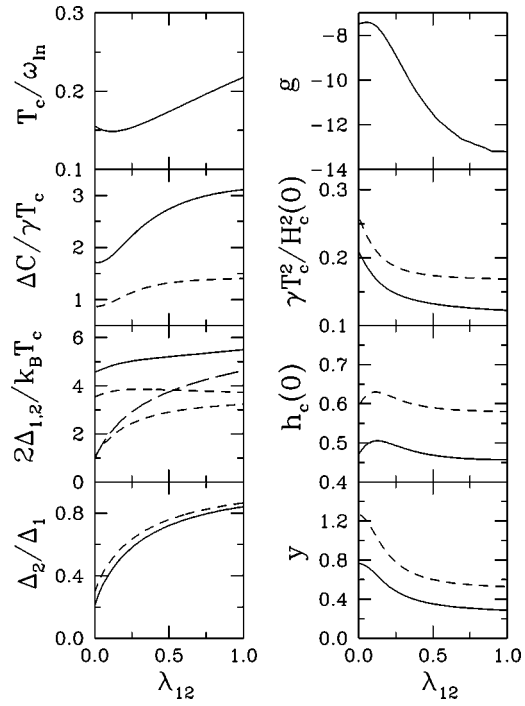

FIG. 8. Various BCS ratios as discussed in the text, shown as a function of λ_{12}, where $\lambda_{21}=\lambda_{12}$ (i.e., $\alpha=1$), $\lambda_{11}=1.3$, and $\lambda_{22}=0.5$. The solid curves are those for the full Eliashberg calculation for a Lorentzian model of $\alpha^2F_{ij}(\omega)$ spectra and the short-dashed curves are for the renormalized BCS formulas developed from the $\lambda^{\theta\theta}$ model and given in the text. For the frame with the gap ratios, the upper gap is given by the solid curve and the lower gap is given by the long-dashed curve, the upper and lower short-dashed curves are for the upper and lower gaps, respectively, in RBCS. The first frame gives the effective T_c/ω_{ln} for the Eliashberg spectrum based on the definition given in the text.

columns were obtained for our Lorentzian spectral density model (Lor.) with $\lambda_{11}=1.3$, $\lambda_{22}=0.5$, $\lambda_{12}=\lambda_{21}=0.2$, and $\mu_{ij}^*=0$. This was devised to have a strong coupling index $T_c/\omega_{ln}\sim 0.15$, which is slightly larger than Pb and well within the range of realistic values for electron-phonon superconductors. It is clear that strong coupling corrections are now even more significant and cannot be ignored in a complete theory.

More information on strong coupling effects as well as on two-band anisotropy is given in Fig. 8, where we show the same BCS ratios as considered in Table I. In all eight frames, we have used our model Lorentzian $\alpha_{ij}^2F(\omega)$ spectra. The solid curves are results of full Eliashberg calculations as a function of $\lambda_{12}=\lambda_{21}$, with λ_{11} fixed at 1.3 and λ_{22} at 0.5. The dashed curves are for comparison and are based on our $\lambda^{\theta\theta}$ formulas, i.e., give renormalized BCS results without use of the strong coupling correction formulas. They, of course, can differ very significantly from one-band universal BCS values because of the two-band anisotropy. We see that these effects can be large and that on comparison between the solid and dashed curves, the strong coupling effects can also be significant. As $\lambda_{12}=\lambda_{21}$ is increased from zero, with λ_{11} and λ_{22} remaining fixed, the T_c increases and this leads to the increase in T_c/ω_{ln} from about 0.15 at $\lambda_{12}=\lambda_{21}=0$ to over 0.2 at

$\lambda_{12}=\lambda_{21}=1$. For all the indices considered here, we note that their values at $T_c/\omega_{\ln}=0.2$ are close to the values that they would have in a one-band case,[1] and the remaining anisotropy in the λ_{ij}'s play only a minor role. (Of course, this is a qualitative statement since it is well known that the shape of $\alpha^2F(\omega)$ for fixed $T_c/\omega_{\ln}$ can also affect somewhat the value of BCS ratios.[1]) This is expected since in this case the fluctuation off the average of any λ_{ij} is becoming smaller. For RBCS, all ratios have returned to the one-band case at $\lambda_{12}=\lambda_{21}=1$ except for y which remains 6% larger. We now comment on select indices separately. The normalized specific heat jump at T_c in the $\lambda^{\theta\theta}$ model is given by formula (32) with $\eta_C=1$. For $\lambda_{12}=\lambda_{21}$ small, $\chi_1^{-1}\simeq 1+O(\overline{\lambda_{12}^2})$ and $\chi_2^{-1}\simeq 0+O(\overline{\lambda_{12}^4})$. These conditions mean that $\Delta C/\gamma T_c$ rises slightly as $\lambda_{12}=\lambda_{21}$ increases, and eventually reaches 1.43. By contrast, the solid curve includes, in addition, strong coupling effects that increase the value of the jump ratio rather rapidly. For $2\Delta_{1,2}/k_BT_c$, the lower gaps have the same value for $\lambda_{12}=\lambda_{21}=0$ as it is determined only by λ_{22}. This is not so for the upper gaps. The dashed curve takes on its BCS value of 3.53, but the solid curve (an Eliashberg calculation) has strong coupling effects as described in Fig. 4. (This means that Δ_2/Δ_1 is smaller for the solid curve as compared to the dashed one in the lower left-hand frame.) As $\lambda_{12}=\lambda_{21}$ increases, the long-dashed and lower short-dashed curves begin to deviate because the former starts to acquire strong coupling corrections of its own through the off-diagonal λ's. While the solid curve also increases, the anisotropy between 1 and 2 decreases. The short-dashed curves show different behavior. The ratio $2\Delta_1/k_BT_c$ starts at 3.53, rises slightly towards 4, before tending towards 3.53 again. Now, the anisotropy between Δ_2 and Δ_1 decreases mainly because Δ_2 itself rises towards 3.53. The behavior of $\gamma T_c^2/H_c^2(0)$ (dashed curve) can be understood from Eq. (38) . While Δ_1/T_c, as we have seen, does change somewhat with $\lambda_{12}=\lambda_{21}$, a more important change is the u^2 factor in the denominator of Eq. (38), which rapidly decreases this ratio towards its BCS value of 0.168 as u increases towards 1. The behavior of $h_c(0)$ given by Eq. (41) is more complex. The numerator in the square root goes towards $1+\alpha^*$, as $u^2\rightarrow 1$, more rapidly than the denominator, which involves the χ's. Here, the numerator and denominator compete and consequently $h_c(0)$ first increases before showing a slow decrease to its BCS value. Finally, y in formula (49) decreases with increasing off-diagonal λ because of the square bracket in the denominator. It is clear from these comparisons between Eliashberg and RBCS calculations that, in general, both strong coupling and anisotropy effects play a significant role in the dimensionless ratios, and both need to be accounted for.

V. THE LIMIT OF NEARLY SEPARATE BANDS

When $\lambda_{12}=\lambda_{21}=0$, there exist two transition temperatures T_{c1} and T_{c2} associated with λ_{11} and λ_{22}, separately, and for several properties, but not all, the superconducting state is the straight sum of the two bands as they would be in isolation. Here, we wish to study how the integration of the two bands proceeds as λ_{12} and/or λ_{21} is switched on. Our first results related to this issue are shown in Fig. 9, which has three frames. The top frame deals with the normalized specific heat $C_S(T)/\gamma T$ as a function of temperature; the middle, the normalized inverse square of the penetration depth $[\lambda_L(0)/\lambda_L(T)]^2$; and the bottom gives the critical field deviation function $D(t)$ of Eq. (35) . In all cases, we have used our Lorentzian model for the spectral densities $\alpha_{ij}^2F(\omega)$ with $\lambda_{11}=1$ and $\lambda_{22}=0.5$ fixed for all curves. The solid curves are for $\lambda_{12}=\lambda_{21}=0.0001$, short-dashed for 0.01, and long-dashed for 0.1. In the top two frames, the two separate transitions are easily identified in the curves with solid line type. Because of the very small value of $\lambda_{12}=\lambda_{21}$, the composite curve is obviously the summation of two subsystems, which are almost completely decoupled. However, already for $\lambda_{12}=\lambda_{21}=0.01$, which remains very small as compared with the value of λ_{11} and even λ_{22}, the second transition (short-dashed curve) becomes significantly smeared. The two subsystems have undergone considerable integration. In particular, the second specific heat jump is rounded, becoming more kneelike. Also, the sharp edge or kink in the solid curve for the superfluid density is gone in the short-dashed curve. Thus, to observe clearly two distinct systems, the off-diagonal λ's need

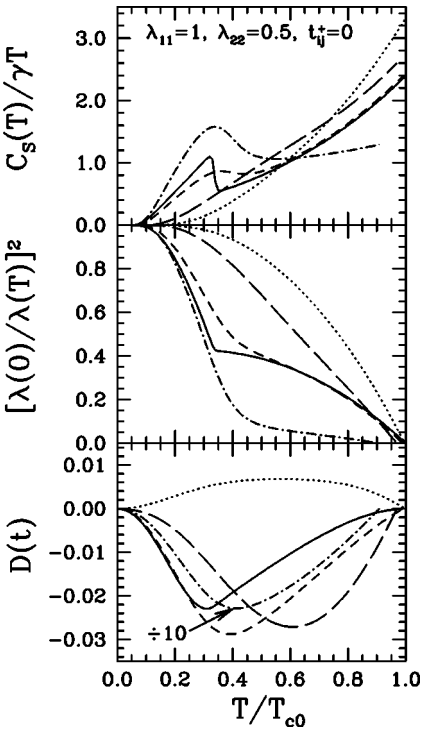

FIG. 9. Upper frame: Specific heat in the superconducting state normalized to the normal state, $C_S(T)/\gamma T$, vs T/T_{c0}, where T_{c0} is the T_c for only the λ_{11} channel, with all others zero. Shown are curves for various off-diagonal λ's with $\lambda_{11}=1$ and $\lambda_{22}=0.5$. Three curves are shown for $\lambda_{12}=\lambda_{21}=0.0001$ (solid), 0.01 (short-dashed), and 0.1 (long-dashed). Also shown are $\lambda_{12}=0.1$ and $\lambda_{21}=0.01$ (i.e., $\alpha=10$) (dot-dashed) and $\lambda_{12}=0.01$ and $\lambda_{21}=0.1$ (i.e., $\alpha=0.1$) (dotted). Middle frame: The superfluid density $[\lambda(0)/\lambda(T)]^2$ vs T/T_{c0} for the same parameters. Lower frame: The deviation function $D(t)$ plotted vs T/T_{c0}. The dot-dashed curve has been divided by 10 from its original value in order to display it on the same scale as the other curves.

to be very small. Once $\lambda_{12}=\lambda_{21}=0.1$ (long-dashed curve), the integration of the two subsystems is very considerable if not complete. This does not mean, however, that superconducting properties become identical to those for an equivalent one-band system. As long as the $\alpha_{ij}^2F(\omega)$ are not all the same, there will be anisotropy and this will change properties as compared with isotropic Eliashberg one-band results. Note that in the solid Eliashberg curve of Fig. 6, a point of inflection remains, as commented on by Golubov *et al.*[17] In the case of the deviation function (lower frame), the solid curve shows a sharp cusp that is related to the lower transition temperature of the decoupled bands but not quite at that value as this function is composed from subtracting $1-(T/T_c)^2$ from $H_c(T)/H_c(0)$. However, two distinct pieces of the curve exist and notably near T_c the curve has a very different curvature from what is normally encountered. In particular, the temperature dependence of the solid curve is concave down at high temperature in contrast to the usual case of concave up. As the bands are coupled through larger and larger interband λ's, the curve moves to a shape more consistent with one-band behavior. However, the curve remains negative due to the anisotropy, while usually strong coupling would drive the curve positive with an overall concave-down curvature,[1] which is illustrated by the dotted curve for which the first band dominates, as we describe below.

The other curves in these figures, dot-dashed and dotted, are for $\alpha=10$ with $\lambda_{12}=0.1$ and $\lambda_{21}=0.01$, and $\alpha=0.1$ with $\lambda_{12}=0.01$ and $\lambda_{21}=0.1$, respectively. For $\alpha=10$, the second band with the smaller of the two diagonal values of λ has 10 times the density of states as compared to band 1 with the larger λ value. This large disparity in density of states can have drastic effects on superconducting properties, and further modify both the observed temperature dependence and the value of the BCS ratios. The second specific heat jump in the dash-dotted curve, although smeared, is quite large as compared with that in the solid or even the dashed curve. Also, it is to be noted that beyond the temperature of the lower maximum in $C_S(T)/\gamma T$, the curve shows only a very modest increase, reflecting the low value of the electronic density of states in band 1, and the ratio of the jump at T_c to the normal state is now quite reduced. The low density of states in band 1 is also reflected in the low value of the penetration depth curve (middle frame, dash-dotted curve) in the temperature region above T_{c2}. Finally, we note that while we have chosen a large value of α for illustration here, MgB_2 has $\alpha=1.37$ which, by the above arguments, would tend to accentuate the features due to the second band.

A very different behavior is obtained when $\alpha=0.1$, for which case the electronic density of states in the second band is reduced by a factor of 10 as compared to the first band. In this case, the dotted curve applies and looks much more like a standard one-band case with very significant strong coupling effects $\Delta C(T_c)/\gamma T_c \simeq 2.4$. The influence of band 2 has been greatly reduced. Finally, we note that the introduction of the off-diagonal elements can change T_c. In particular, the dot-dashed curve ends at a considerably reduced value of critical temperature as compared with the other curves. This is consistent with Fig. 1, where we saw that increasing λ_{12} for small values of λ_{21} decreases T_c. On the other hand, for the dotted curve for which values of λ_{12} and λ_{21} are interchanged as compared to the dash-dotted curve, T_c is hardly affected because λ_{12} is small and it is this parameter that affects T_c more. The two parameters λ_{12} and λ_{21} do not play the same role in T_c or for that matter in the integration process of the two bands. This is made clear in Fig. 10, which deals only with the penetration depth. What is shown are the separate contributions to the superfluid density coming from the two bands. In all cases, $\lambda_{11}=1$ and $\lambda_{22}=0.5$. In the top frame, $\lambda_{12}=0.0001$ and λ_{21} is varied. It is clear that as λ_{21} is increased, the superfluid density associated with the second band remains significant even above the second transition temperature T_{c2}, which is well defined in the solid curve. This is the opposite behavior of what is seen in the lower frame where λ_{21} remains at 0.0001 and λ_{12} is increased. In this case, T_c changes significantly but the superfluid density associated with the second band remains negligible above T_{c2}. Note finally that the relative size of the superfluid density in each band will vary with α and v_{Fi}, neither of which have been properly accounted for in this figure, as we wished to illustrate solely the effect of λ_{12} and λ_{21} on the issue of integration of the bands and modification of T_c.

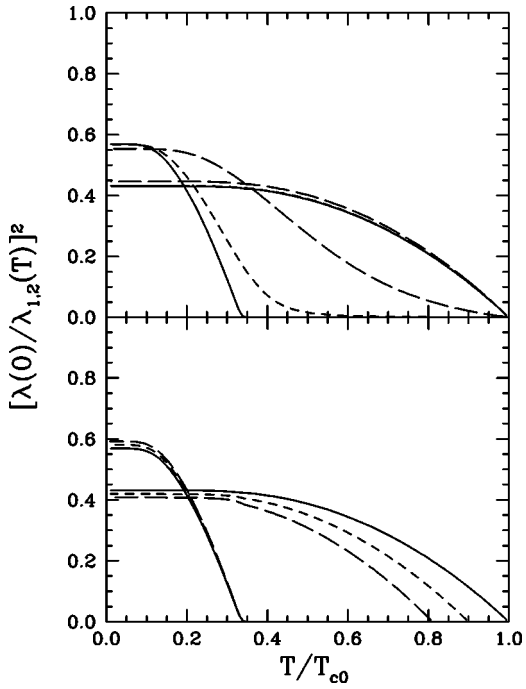

FIG. 10. Upper frame: Individual contributions from each band to the superfluid density $[\lambda(0)/\lambda_{1,2}(T)]^2$ as a function of T/T_{c0}, where T_{c0} is the T_c for the λ_{11} channel alone, with all others zero. Shown are curves for various off-diagonal λ_{21} with $\lambda_{11}=1$, $\lambda_{22}=0.5$, and $\lambda_{12}=0.0001$. The three pairs of curves are for $\lambda_{21}=0.0001$ (solid), 0.01 (short-dashed), and 0.1 (long-dashed). The curves, which go to zero at a lower temperature, correspond to $[\lambda(0)/\lambda_2(T)]^2$, while those that go to zero close to 1 are for $[\lambda(0)/\lambda_1(T)]^2$. Lower frame: Now the λ_{21} is held fixed at 0.0001 and the λ_{12} is varied. The three pairs of curves are for $\lambda_{12}=0.0001$ (solid), 0.1 (short-dashed), and 0.2 (long-dashed). Here, the ratio of the density of states α has been taken to be 1 for convenience of illustrating the curves on the same scale.

The changes, with the off-diagonal elements λ_{12} and λ_{21}, in the temperature dependence of the upper and lower gaps

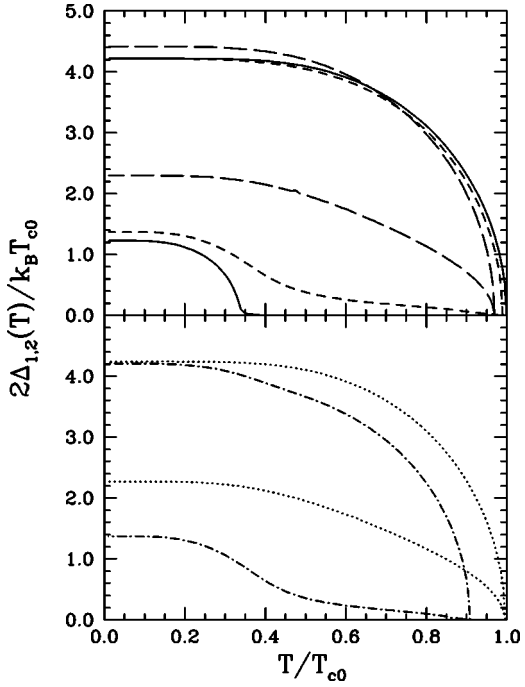

FIG. 11. Upper frame: Upper and lower gap ratios, $2\Delta_{1,2}/k_BT_{c0}$, vs T/T_{c0}, where T_{c0} is the T_c for the λ_{11} channel alone, with all λ's zero. Shown are curves for various off-diagonal λ's with $\lambda_{11}=1$ and $\lambda_{22}=0.5$. Three pairs of curves are shown for $\lambda_{12}=\lambda_{21}=0.0001$ (solid), 0.01 (short-dashed), and 0.1 (long-dashed). Lower frame: Same as for upper frame except now are shown: $\lambda_{12}=0.1$ and $\lambda_{21}=0.01$ (i.e., $\alpha=10$) (dot-dashed) and $\lambda_{12}=0.01$ and $\lambda_{21}=0.1$ (i.e., $\alpha=0.1$) (dotted).

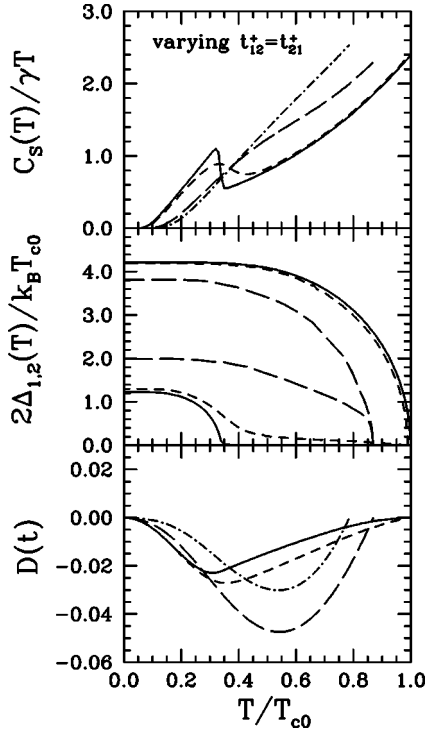

FIG. 12. Top frame: Specific heat in the superconducting state normalized to the normal state, $C_S(T)/\gamma T$, vs T/T_{c0}, where T_{c0} is the T_c for the pure case. Here, $\lambda_{11}=1$, $\lambda_{22}=0.5$, and $\lambda_{12}=\lambda_{21}=0.0001$. Shown are curves for varying $t_{12}^+=t_{21}^+$ equal to 0.0 (solid), 0.01 (short-dashed), 0.2 (long-dashed), and 0.5 (dot-dashed) in units of T_{c0}. Notice that the value of the jump at T_c first dips and then rises with impurity scattering. Middle frame: $2\Delta_{1,2}/k_BT_{c0}$ vs T/T_{c0}. The upper three curves correspond to $2\Delta_1/k_BT_{c0}$ and the lower three to $2\Delta_2/k_BT_{c0}$, with the curves labeled the same way as in the upper frame. Only the first three impurity cases are shown for clarity. The other progresses in the same manner with the T_c reducing further and the gaps moving closer to a common value. Bottom frame: The deviation function $D(t)$ vs T/T_{c0}, again with the curves labeled the same way as in the top frame.

are closely correlated with those just described for the superfluid density. This is documented in Fig. 11, which has two frames. In all cases $\lambda_{11}=1$ and $\lambda_{22}=0.5$. In the top frame, $\lambda_{12}=\lambda_{21}$ equal to 0.0001 (solid), 0.01 (short-dashed), and 0.1 (long-dashed). The various pairs of curves apply to the upper and lower gap ratios. Note the long tails in the short-dashed curve (lower gap), still small but extending to $T=T_c$. For the long-dashed curve, the lower and upper gaps now have very similar temperature dependences, but these are not yet identical to BCS. We have already seen in Fig. 7, for the specific case of MgB_2, that the lower gap falls below BCS at temperatures above $T/T_c\simeq 0.7$, which is expected when it is viewed as an evolution out of two separate gaps, with two T_c values, due to increasing the off-diagonal coupling. In the lower frame, we show results for $\alpha=10$ (dot-dashed) and $\alpha=0.1$ (dotted). Again, as expected, the two dash-dotted curves show distinct temperature dependences, while for the dotted curves they are very similar.

A very similar story emerges when interband impurity scattering is considered. Results are given in Figs. 12 and 13. Figure 12 has three frames. Here, $\lambda_{11}=1$, $\lambda_{22}=0.5$, and $\lambda_{12}=\lambda_{21}=0.0001$, with our Lorentzian electron-phonon spectral functions $\alpha_{ij}^2F(\omega)$ described previously. The top frame deals with the temperature dependence of the normalized superconducting state electronic specific heat $C_S(T)/\gamma T$. The middle frame gives the gap ratios of Δ_1 and Δ_2 and thus the curves come in pairs, with $\Delta_1>\Delta_2$. The bottom frame shows the deviation function $D(t)$ for the thermodynamic critical magnetic field. What is varied in the various curves is the interband impurity scattering rate $t_{12}^+=t_{21}^+$ (taken to be equal in value, i.e., $\alpha=1$). The solid curve, which clearly shows two transitions, is for $t_{12}^+=0$. It is to be noted first, that in all cases, off-diagonal impurity scattering changes the value of the critical temperature, reducing it to less than 0.8 of its pure value in the case of the dot-dashed curve. This decrease in T_c does not translate, however, into a steady decrease in the specific heat jump at T_c. We see that while the jump initially decreases with increasing $t_{12}^+=t_{21}^+$; eventually it increases and is largest for the dot-dashed curve. Both Watanabe and Kita[30] and Mishonov *et al.*,[31] using only an unrenormalized BCS model, find an increase with impurity scattering and no initial decrease as is found in the full Eliashberg calculation. This is a clear illustration that, at minimum, a renormalized BCS formula needs to be used to capture the qualitative trend, and full Eliashberg theory is required if one wishes to be quantitative. It is also clear that as interband impurity scattering increases, the jump in the specific heat at the second transition, seen in the solid curve,

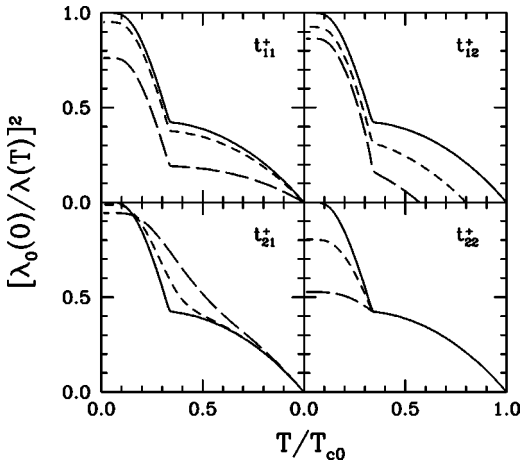

FIG. 13. Effect of impurity scattering on the superfluid density $[\lambda_0(0)/\lambda(T)]^2$ plotted vs T/T_{c0}, where T_{c0} and $\lambda_0(0)$ are for the pure case. Each frame shows the effect of the different type of impurity scattering, keeping all other impurity terms equal to zero. The spectrum parameters are $\lambda_{11}=1$, $\lambda_{22}=0.5$, and $\lambda_{12}=\lambda_{21}=0.0001$. The solid curve in all cases is for the pure case of $t_{ij}^+=0$. In the upper left frame: $t_{11}^+/T_{c0}=0.2$ (short-dashed) and 2.0 (long-dashed). In the upper right frame: $t_{12}^+/T_{c0}=0.2$ (short-dashed) and 0.4 (long-dashed). In the lower left frame: $t_{21}^+/T_{c0}=0.02$ (short-dashed) and 0.1 (long-dashed). In the lower right frame: $t_{22}^+/T_{c0}=0.2$ (short-dashed) and 2.0 (long-dashed).

is rapidly washed out and little remains of this anomaly in the dot-dashed curve. Even the long-dashed curve shows little structure in this region, in analogy to what we found to hold for the case of increasing the off-diagonal electron-phonon elements. Note, however, there remains a point of inflection that has moved to higher temperature. Such a shift of the inflection point can also be brought about by increasing the off-diagonal λ's as seen in Fig. 9.

The temperature dependence of the gap ratios (middle frame of Fig. 12) also mirror what we found in Fig. 11. The dashed curves exhibit quite distinct temperature dependences between Δ_1 and Δ_2, while this is no longer the case for the pair of long-dashed curves. Note that, as compared to the solid curve, the anisotropy in the gaps for the long-dashed curve has been reduced considerably. The upper gap has decreased and the lower increased even more. The washing out of the gap anisotropy by off-diagonal impurity scattering is expected and has been studied theoretically[33,53] and experimentally.[54] For carbon doping, the gaps are seen to merge at about 13% for which T_c has been reduced to about 20 K with the large gap reducing to its BCS value and the smaller gap moving upwards only very little in contrast to our model calculations for which the lower gap changes relatively more and isotropy is reached at about a 30% reduction in T_c. Of course, as one dopes, the electronic density of states and the electron-phonon parameters also change,[55] and one needs to include these in addition to any interband scattering.

Finally, the effect of interband ordinary impurity scattering on the deviation function, shows a behavior similar to that found for paramagnetic impurities in one-band superconductors.[35] Initially, as in the other properties, the impurities smear the structure related to the second transition temperature (in this case the cusp feature in the solid curve), and once the two bands are fairly well integrated, then like paramagnetic impurities, the effect here is to keep the minimum at the same temperature but change its value. A key difference though is that, in the case of paramagnetic impurities in one-band superconductors, the extremum in the curve moves from positive (and strong coupling) to negative (and weak coupling) because the gap is being reduced towards zero. Here, with the two bands, the impurities do not reduce T_c, and hence the gap, to zero, but rather to a finite value related to the washing out of the anisotropy between the two bands, and hence the extremum in this case will move from negative (where it is positioned due to large anisotropy) to smaller values, reflecting this.

Next we turn to the results given in Fig. 13, which shows the temperature dependence of the superfluid density for various values of impurity parameters. Again, $\lambda_{11}=1$, $\lambda_{22}=0.5$, and $\lambda_{12}=\lambda_{21}=0.0001$ with the Lorentzian spectra. What is illustrated in these four frames is how very different the effect of t_{11}^+, t_{22}^+, t_{12}^+, and t_{21}^+ are. The solid curve is for reference and is the pure case. Once again, for the case of varying t_{12}^+ and t_{21}^+, we have violated the constraint that their ratio must be fixed by the ratio of the density of states. This we can do theoretically to decouple and, therefore, illustrate the effects of these different scattering channels, but in real systems, they would be constrained and the net result would be a combination of the effects from both channels. The top left frame shows the effect on the superfluid density of increasing the impurity scattering in the first band (intraband scattering). Such impurities reduce the superfluid density in band 1 while leaving band 2 unaltered. In the lower right-hand frame it is the superfluid density in the second band that is reduced, leaving the first unchanged. T_c is unaffected by intraband impurity scattering in isotropic *s*-wave superconductors due to Anderson's theorem. The top right-hand frame shows that increasing t_{12}^+ reduces the critical temperature as well as reduces the superfluid density in band one without, however, having much effect on the second band. The kink associated with the rise of the second band is hardly changed as t_{12}^+ is not the integrating variable, rather it is t_{21}^+ which integrates the bands rapidly as seen in the lower left-hand frame. However, in this case, the critical temperature is hardly changed and there is little change to the curve above $T/T_{c0}\simeq 0.7$.

VI. THE LIMIT OF PURE OFF-DIAGONAL COUPLING

While the two-band nature in MgB_2, driven by the electron-phonon interaction, is well established, there have been many reports of possible two-band superconductivity in other systems, including the conventional *A*15 compound Nb_3Sn.[56] With $T_c=18$ K and a main gap $2\Delta_M\sim 4.9T_c$, there is specific heat evidence for a second gap at $0.8T_c$. Other systems are $NbSe_2$,[57] Y_2C_3 and La_2C_3,[58] and possibly a second nonsuperconducting band in $CeCoIn_5$.[59] In the triplet spin state superconductor Sr_2RuO_4,[60] a small gap is induced in the second band. As two-band superconductivity is likely to be a widespread phenomenon, not confined to electron-phonon systems, it seems appropriate to investigate further

an extended range of parameter space for the λ_{ij}'s and in particular the possibility that the off-diagonal elements are the dominant mechanism for superconductivity.

In the limit of pure off-diagonal coupling, where $\lambda_{11}=\lambda_{22}=0$, Eq. (12) for the coupling A, which determines T_c from Eq. (11) , simplifies to

$$A=\frac{1}{\sqrt{\overline{\lambda}_{12}\overline{\lambda}_{21}}}, \tag{51}$$

and the ratio of the gap to T_c given in Eq. (21) becomes

$$\frac{2\Delta_1}{k_BT_c}=3.54\ \exp\left[A-\frac{u}{\overline{\lambda}_{21}}\right]. \tag{52}$$

The ratio $\overline{\lambda}_{12}/\overline{\lambda}_{21}=\alpha^*$ can be taken $\geqslant 1$ and Eq. (20) for the gap anisotropy $u=\Delta_2/\Delta_1$ written as

$$\alpha^* u^2-1=\frac{\sqrt{\alpha^*}}{A}u\ \ln u. \tag{53}$$

This equation gives u in terms of α^* and A. Since by its definition $0<u\leqslant 1$, $u\ \ln u$ is negative so a condition on obtaining a solution of Eq. (53) is that

$$\alpha^* u^2-1<0 \quad \text{or} \quad \alpha^*\leqslant\frac{1}{u^2}. \tag{54}$$

For a trial solution of $u=0.1$, this would give $1<\alpha^*<100$. For $\alpha^*=60$, as an example, $A=4.46$ and $2\Delta_1/k_BT_c\simeq 9.7$, which is very large. This occurs for $T_c/\omega_{\ln}\sim 10^{-2}$, using $\ln(1.13\omega_{\ln}/T_c)=A$, which is in the weak coupling regime. However, to achieve an upper gap ratio value greater than 11 or so, will correspond an unrealistically small value of $T_c/\omega_{\ln}$ (of order 10^{-10}, for example). In Fig. 14, we show results in the upper frame for $2\Delta_{1,2}/k_BT_c$ versus λ_{12} for various λ_{21} values. In the lower frame, we show u versus λ_{12}. The difference between Fig. 14 and Fig. 3 shows that large values of $2\Delta_1/k_BT_c$ are more naturally obtained in the pure off-diagonal regime and are associated as well with small values of u and the weak coupling regime. This latter feature implies that there will be no further strong coupling corrections to an already large gap ratio. We have also calculated the thermodynamics and superfluid density in this regime, for a range of parameters, but have found these properties to show quite ordinary behavior and have discovered no new physics. For the sake of brevity, we present none of these results but instead note that in this limit the χ's are

$$\chi_1=\frac{1}{2}\left[1+\frac{\overline{\lambda}_{21}}{\overline{\lambda}_{12}}\right]=\frac{1}{2}\left[1+\frac{1}{\alpha^*}\right], \tag{55}$$

$$\chi_2=\frac{1}{2}\left[1+\frac{\overline{\lambda}_{12}}{\overline{\lambda}_{21}}\right]=\frac{1}{2}(1+\alpha^*), \tag{56}$$

with $\alpha^*=\overline{\lambda}_{12}/\overline{\lambda}_{21}$, and hence, the various dimensionless ratios are

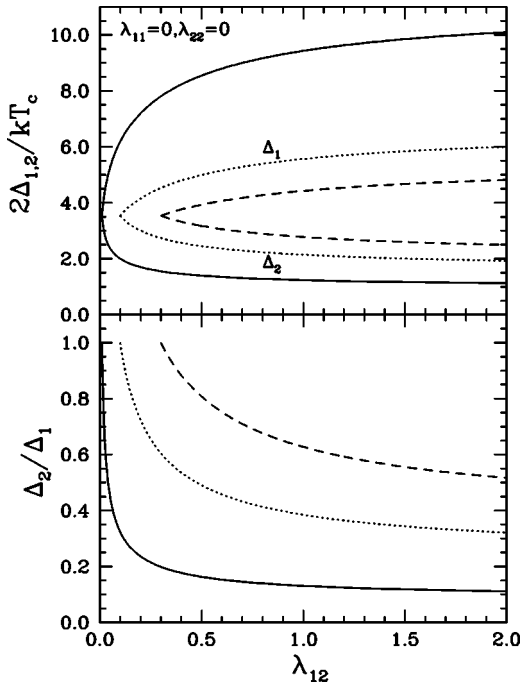

FIG. 14. Upper frame: Gap ratios for the upper $(2\Delta_1/k_BT_c)$ and lower gap $(2\Delta_2/k_BT_c)$ as a function of λ_{12} for varying λ_{21}: 0.01 (solid), 0.1 (dotted), and 0.3 (dashed). Here, $\lambda_{11}=0$, $\lambda_{22}=0$. This is for comparison with Suhl *et al.* (Ref. 9). Lower frame: Gap anisotropy, $u=\Delta_2/\Delta_1$, vs λ_{12} for the same parameters and curve labels as the upper frame. Note that $\lambda_{12}\geqslant\lambda_{21}$ is plotted. With $\lambda_{12}<\lambda_{21}$, the roles are simply reversed with $1\leftrightarrow 2$ and Δ_2 would become the large gap, etc.

$$\frac{\Delta C}{\gamma T_c}=1.43\left[\frac{4\alpha^*}{(1+\alpha^*)^2}\right], \tag{57}$$

and

$$h_c(0)=\frac{\Delta_1}{T_c}\frac{1}{\pi}\sqrt{\frac{7\zeta(3)}{32}}(1+\alpha^*)\sqrt{\frac{1+\alpha u^2}{\alpha+\alpha^{*2}}}, \tag{58}$$

and

$$\frac{y_L'(0)}{|y_L(T_c)|T_c}=\frac{1}{4}\frac{(1+\alpha\beta)(1+\alpha^*)}{\alpha^*+\beta\alpha}, \tag{59}$$

where $\beta=v_{F2}^2(1+\lambda_{12})/v_{F1}^2(1+\lambda_{21})$. The ratio for the zero-temperature critical field of Eq. (38) does not change its form and so is not repeated here. These ratios behave, qualitatively, no differently from what we found in Sec. III. A difference worth noting is the following. In linear order, the effect of interband impurity scattering on T_c takes the form (16)–(18):

$$\frac{\Delta T_c}{T_{c0}}=-\frac{\pi^2}{8}\rho_{12}^{\pm}\left[1\mp\sqrt{\frac{\overline{\lambda}_{21}}{\overline{\lambda}_{12}}}\right]^2, \tag{60}$$

which is always negative and larger for paramagnetic than for normal impurities. It can also be very large for $\rho_{12}^{\pm}\gg 1$. This is another distinction between pure off-diagonal cou-

pling and MgB_2, for example. In obtaining Eq. (60), we have used the fact that $\bar{\lambda}_{12}/\bar{\lambda}_{21}=\rho_{12}/\rho_{21}$ and $\underline{\lambda}_{12}/\underline{\lambda}_{21}>1$.

VII. CONCLUSIONS

We have calculated the thermodynamics, gap anisotropy and penetration depth for a two-band Eliashberg superconductor. For the parameters appropriate to MgB_2, which are obtained from first-principle band structure calculations of the electron-phonon spectral functions, we find good agreement with the existing experimental data. We reduce the Eliashberg equations to a renormalized BCS form by application of the two-square-well approximation. Comparison of these results with those from the full Eliashberg equations allows us to determine strong coupling corrections, which we find to be significant in MgB_2. When the parameters for the electron-phonon interaction are moved away from those specific to MgB_2, the strong coupling corrections can become much larger, and superconducting properties reflect this fact, as well as the change in anisotropy between the bands. Within the $\lambda^{\theta\theta}$ approximation, we derive simple analytic expressions for the various dimensionless BCS ratios that would be universal in the one-band case, but are not in the two-band one. They depend on the anisotropy and particularly on the ratio of the electronic density of states in the two bands. The anisotropy in the ratio of the two gaps at zero temperature is investigated and is found to increase as λ_{22} is reduced and made repulsive, in which case the existence of superconductivity in the first band, and the off-diagonal coupling to it, induces a gap in a band, which would, on its own, not be superconducting.

We have paid particular attention to the limit of nearly decoupled bands, i.e., small interband coupling, with the superconductivity originating from λ_{11} and λ_{22} in the first and second band, respectively. When $\lambda_{12},\lambda_{21}\rightarrow 0$, there are two transitions at T_{c1} and T_{c2} and two specific heat jumps. As the interband coupling is turned on, the two bands become integrated and the second transition smears. We have found that the two parameters, λ_{12} and λ_{21}, have very different effects on the smearing of the second transition and on T_c. λ_{12} largely modifies T_c, reducing it, whereas λ_{21} alters the lower-temperature region around the second transition. Only very small values of λ_{21}, as compared with λ_{11} and λ_{22}, are needed to cause large changes in the region around T_{c2}. It was found that a small amount of interband impurity scattering can also significantly smear the second transition, and so reduce the distinction between the two bands. However, even when the two bands are well integrated and a sharp second transition is no longer easily discernible, this does not imply that the superconducting properties become those of a one-band superconductor. Anisotropy remains and this affects properties.

In view of the possible widespread occurrence of two-band superconductivity, even for systems with exotic mechanisms not necessarily due to the electron-phonon interaction, we deemed it of interest to consider the case of zero intraband coupling, $\lambda_{11}=\lambda_{22}=0$, with superconductivity due only to the interband λ_{12} and λ_{21}, which need not have the same value. When these are very different, the resulting gaps are quite different from each other and the ratio of Δ_1 to T_c can become large particularly in the weak coupling limit. This is a distinguishing feature of pure off-diagonal coupling. Another distinguishing feature is the possibility of a rapid reduction of T_c towards zero by interband impurity scattering, as compared with the case for which the diagonal elements play the leading role.

ACKNOWLEDGMENTS

E.J.N. acknowledges funding from NSERC, the Government of Ontario, and the University of Guelph. J.P.C. acknowledges support from NSERC and the CIAR. In addition, we thank E. Schachinger and J. Wei for helpful discussions.

[1] J. P. Carbotte, Rev. Mod. Phys. **62**, 1027 (1990).
[2] The Pb $\alpha^2F(\omega)$ is given by W. L. McMillan and J. M. Rowell, in *Superconductivity*, edited by R. D. Parks (Marcel Dekker, New York, 1969), Vol. 1, p. 601.
[3] F. Marsiglio and J. P. Carbotte, in *The Physics of Conventional and Unconventional Superconductors*, edited by K. H. Bennemann and J. B. Ketterson (Springer Verlag, Berlin, 2003), Vol. 1, p. 233.
[4] J. M. Daams and J. P. Carbotte, J. Low Temp. Phys. **43**, 263 (1981).
[5] P. Tomlinson and J. P. Carbotte, Phys. Rev. B **13**, 4738 (1976).
[6] H. K. Leung, J. P. Carbotte, and C. R. Leavens, J. Low Temp. Phys. **24**, 25 (1976).
[7] See the book *Anisotropy Effects in Superconductors*, edited by H. Webber (Plenum Press, New York, 1977).
[8] H. G. Zarate and J. P. Carbotte, Phys. Rev. B **27**, 194 (1983).
[9] H. Suhl, B. T. Matthias, and L. R. Walker, Phys. Rev. Lett. **3**, 552 (1959).
[10] Some further examples of two-band work from the past are T. Soda and Y. Wada, Prog. Theor. Phys. **36**, 1111 (1996); C. C. Sung and V. K. Wong, J. Phys. Chem. Solids **28**, 1933 (1967); W. S. Chow, Phys. Rev. **172**, 467 (1968); R. H. Burkel and W. S. Chow, Phys. Rev. B **3**, 779 (1971); V. A. Moshalenko, A. M. Ursu, and N. I. Botoshan, Phys. Lett. **44A**, 183 (1973); N. Schopohl and K. Scharnberg, Solid State Commun. **22**, 371 (1977).
[11] P. Entel and D. Rainer, J. Low Temp. Phys. **23**, 511 (1976).
[12] P. Entel, Z. Phys. B **24**, 263 (1976); **23**, 321 (1976).
[13] J. Nagamatsu, N. Nakagawa, T. Muranaka, Y. Zenitani, and J. Akimitsu, Nature (London) **410**, 63 (2001).
[14] A. Y. Liu, I. I. Mazin, and J. Kortus, Phys. Rev. Lett. **87**, 087005 (2001).
[15] H. J. Choi, D. Roundy, H. Sun, M. L. Cohen, and S. G. Louie, Phys. Rev. B **66**, 020513 (2002).
[16] H. J. Choi, D. Roundy, H. Sun, M. L. Cohen, and S. G. Louie, Nature (London) **418**, 758 (2002).

[17] A. A. Golubov, A. Brinkman, O. V. Dolgov, J. Kortus, and O. Jepsen, Phys. Rev. B **66**, 054524 (2002).
[18] A. Brinkman, A. A. Golubov, H. Rogalla, O. V. Dolgov, J. Kortus, Y. Kong, O. Jepsen, and O. K. Andersen, Phys. Rev. B **65**, 180517(R) (2002).
[19] A. A. Golubov, J. Kortus, O. V. Dolgov, O. Jepsen, Y. Kong, O. K. Andersen, B. J. Gibson, K. Ahn, and R. K. Kremer, J. Phys.: Condens. Matter **14**, 1353 (2002).
[20] J. M. An and W. E. Pickett, Phys. Rev. Lett. **86**, 4366 (2001).
[21] I. I. Mazin, O. K. Andersen, O. Jepsen, O. V. Dolgov, J. Kortus, A. A. Golubov, A. B. Kuz'menko, and D. van der Marel, Phys. Rev. Lett. **89**, 107002 (2002).
[22] I. I. Mazin and V. P. Antropov, Physica C **385**, 49 (2003).
[23] I. K. Yanson, cond-mat/0405246 (unpublished).
[24] O. V. Dolgov, R. S. Gonnelli, G. A. Ummarino, A. A. Golubov, S. V. Shulga, and J. Kortus, Phys. Rev. B **68**, 132503 (2003).
[25] Y. Wang, T. Plackowski, and A. Junod, Physica C **355**, 179 (2001); A. Junod, Y. Wang, F. Bouquet, and P. Toulemonde, in *Studies of High Temperature Superconductors*, edited by A. V. Narlikar (Nova Publishers, Commack, NY, 2002), Vol. 38, p. 179.
[26] C. P. Moca, Phys. Rev. B **65**, 132509 (2002).
[27] P. B. Allen and R. C. Dynes, Phys. Rev. B **12**, 905 (1975).
[28] P. B. Allen and B. Mitrović, in *Solid State Physics*, edited by H. Ehrenreich, F. Seitz, and D. Turnbull (Academic, New York, 1982), Vol. 37, p. 1.
[29] E. J. Nicol, J. P. Carbotte, and T. Timusk, Phys. Rev. B **43**, 473 (1991).
[30] K. Watanabe and T. Kita, cond-mat/0401410 (unpublished).
[31] T. M. Mishonov, E. S. Penev, J. O. Indekeu, and V. L. Pokrovsky, Phys. Rev. B **68**, 104517 (2003).
[32] B. Mitrović, Eur. Phys. J. B **38**, 451 (2004).
[33] A. A. Golubov and I. I. Mazin, Phys. Rev. B **55**, 15146 (1997).
[34] B. Mitrović, J. Phys.: Condens. Matter **16**, 9013 (2004).
[35] E. Schachinger, J. M. Daams, and J. P. Carbotte, Phys. Rev. B **22**, 3194 (1980).
[36] B. Mitrović, H. G. Zarate, and J. P. Carbotte, Phys. Rev. B **29**, 184 (1984).
[37] J. Wei (private communication).
[38] M. Iavarone, G. Karapetrov, A. E. Koshelev, W. K. Kwok, G. W. Crabtree, D. G. Hinks, W. N. Kang, Eun-Mi Choi, Hyun Jung Kim, Hyeong-Jin Kim, and S. I. Lee, Phys. Rev. Lett. **89**, 187002 (2002).
[39] F. Marsiglio and J. P. Carbotte, Phys. Rev. B **33**, 6141 (1986).
[40] F. Bouquet, R. A. Fisher, N. E. Phillips, D. G. Hinks, and J. D. Jorgensen, Phys. Rev. Lett. **87**, 047001 (2001).
[41] B. B. Jin, N. Klein, W. N. Kang, H.-J. Kim, E.-M. Choi, S.-I. Lee, T. Dahm, and K. Maki, Phys. Rev. B **66**, 104521 (2002).
[42] F. Manzano, A. Carrington, N. E. Hussey, S. Lee, A. Yamamoto, and S. Tajima, Phys. Rev. Lett. **88**, 047002 (2002).
[43] Ch. Niedermayer, C. Bernhard, T. Holden, R. K. Kremer, and K. Ahn, Phys. Rev. B **65**, 094512 (2002).
[44] R. S. Gonnelli, D. Daghero, G. A. Ummarino, V. A. Stepanov, J. Jun, S. M. Kazakov, and J. Karpinski, Phys. Rev. Lett. **89**, 247004 (2002).
[45] P. Szabó, P. Samuely, J. Kačmarčík, T. Klein, J. Marcus, D. Fruchart, S. Miraglia, C. Marcenat, and A. G.M. Jansen, Phys. Rev. Lett. **87**, 137005 (2001).
[46] F. Giubileo, D. Roditchev, W. Sacks, R. Lamy, D. X. Thanh, J. Klein, S. Miraglia, D. Fruchart, J. Marcus, and Ph. Monod, Phys. Rev. Lett. **87**, 177008 (2001).
[47] H. Schmidt, J. F. Zasadzinski, K. E. Gray, and D. G. Hinks, Phys. Rev. Lett. **88**, 127002 (2002).
[48] M. Putti, M. Affronte, P. Manfrinetti, and A. Palenzona, Phys. Rev. B **68**, 094514 (2003).
[49] F. Bouquet, Y. Wang, R. A. Fischer, D. G. Hinks, J. D. Jorgensen, A. Junod, and N. E. Phillips, Europhys. Lett. **56**, 856 (2001).
[50] H. D. Yang, J.-Y. Lin, H. H. Li, F. H. Hsu, C. J. Liu, S.-C. Li, R.-C. Yu, and C.-Q. Jin, Phys. Rev. Lett. **87**, 167003 (2001).
[51] B. Kang, H.-J. Kim, M.-S. Park, K.-H. Kim, and S.-I. Lee, Phys. Rev. B **69**, 144514 (2004).
[52] Note that in implementing the $\lambda^{\theta\theta}$ model with a finite μ_{ij}^*, in principle, one cannot use the same μ_{ij}^* as those used in the Eliashberg calculation as the Eliashberg μ_{ij}^* depend on the high frequency cutoff ω_c, which is 750 meV in our calculations. The $\lambda^{\theta\theta}$ model is based on modeling the frequency dependent gap function by a constant up to some cutoff that is on the scale of the phonon energies. Typically, an appropriate cutoff might be the maximum phonon frequency or the frequency beyond which the phonon spectrum suddenly drops to small values, as this will be reflected in the gap function by a sudden drop with the gap function going negative. Thus, to maximize the effectiveness of this approximation to mimic the behavior of the gap function, one might use $\omega_o = 75$ meV [as has Mitrović (Ref. 34)] as a major peak in the phonon spectra occurs at this energy, after which it drops to small values. The new $\mu_{ij}^*(\omega_o)$ for the RBCS calculations would then be found from the matrix equation $\hat{\mu}^*(\omega_o) = [1 + \hat{\mu}^*(\omega_c)\ln(\omega_c/\omega_o)]^{-1}\hat{\mu}^*(\omega_c)$ (Ref. 34). For simplicity, we have used the Eliashberg μ^*'s in our calculations for Table I, as we have found that for varying μ^*, the values do not change very much and hardly at all in some cases, and our goal is only to provide a rough estimate of the strong coupling corrections in relation to RBCS.
[53] S. C. Erwin and I. I. Mazin, Phys. Rev. B **68**, 132505 (2003).
[54] R. S. Gonnelli, D. Daghero, G. A. Ummarino, A. Calzolari, Valeria Dellaroca, V. A. Stepanov, S. M. Kazakov, J. Jun, and J. Karpinski, cond-mat/0407267 (unpublished); cond-mat/0407265 (unpublished).
[55] G. A. Ummarino, R. S. Gonnelli, S. Massidda, and A. Bianconi, Physica C **407**, 121 (2004).
[56] V. Guritanu, W. Goldacker, F. Bouquet, Y. Wang, R. Lortz, G. Doll, and A. Junod, cond-mat/0403590 (unpublished).
[57] E. Boaknin, M. A. Tanatar, J. Paglione, D. G. Hawthorn, R. W. Hill, F. Ronning, M. Sutherland, L. Taillefer, J. Sonier, S. M. Hayden, and J. W. Brill, cond-mat/0304499 (unpublished).
[58] I. A. Sergienko, cond-mat/0406527 (unpublished).
[59] M. A. Tanatar *et al.* (private communication).
[60] A. P. Mackenzie and Y. Maeno, Rev. Mod. Phys. **75**, 657 (2003).